

RECEIVED: January 23, 2024

REVISED: February 28, 2024

ACCEPTED: February 29, 2024

PUBLISHED: March 21, 2024

Chiral magnetic waves in strongly coupled Weyl semimetals

Yongjun Ahn ^{a,b,c} Matteo Baggioli ^{a,b,c} Yan Liu ^{d,e} and Xin-Meng Wu ^{a,b,c,*}

^a*School of Physics and Astronomy, Shanghai Jiao Tong University, Shanghai 200240, China*

^b*Wilczek Quantum Center, School of Physics and Astronomy, Shanghai Jiao Tong University, Shanghai 200240, China*

^c*Shanghai Research Center for Quantum Sciences, Shanghai 201315, China*

^d*Center for Gravitational Physics, Department of Space Science, Beihang University, Beijing 100191, China*

^e*Peng Huanwu Collaborative Center for Research and Education, Beihang University, Beijing 100191, China*

E-mail: yongjunahn@sjtu.edu.cn, b.matteo@sjtu.edu.cn, yanliu@buaa.edu.cn, xinmeng.wu@sjtu.edu.cn

ABSTRACT: Propagating chiral magnetic waves (CMW) are expected to exist in chiral plasmas due to the interplay between the chiral magnetic and chiral separation effects induced by the presence of a chiral anomaly. Unfortunately, it was pointed out that, because of the effects of electric conductivity and dissipation, CMW are overdamped and therefore their signatures are unlikely to be seen in heavy-ion collision experiments and in the quark gluon plasma. Nonetheless, the chiral anomaly plays a fundamental role in Weyl semimetals and their anomalous transport properties as well. Hence, CMW could be potentially observed in topological semimetals using table-top experiments. By using a holographic model for strongly coupled Weyl semimetals, we investigate in detail the nature of CMW in presence of Coulomb interactions and axial charge relaxation and estimate whether, and in which regimes, CMW could be observed as underdamped collective excitations in topological materials.

KEYWORDS: Holography and Condensed Matter Physics (AdS/CMT), Holography and Hydrodynamics

ARXIV EPRINT: [2401.07772](https://arxiv.org/abs/2401.07772)

*Corresponding author.

Contents

1	Introduction	1
2	Hydrodynamics of chiral magnetic waves in Dirac and Weyl semimetals	3
3	Magnetic field effects on holographic Weyl semimetals	7
3.1	The solution in the probe limit	7
3.2	Magnetic field effects on the phase diagram	9
3.3	Axial charge relaxation time	10
4	Coulomb interactions in the holographic Weyl semimetal model	13
5	Chiral magnetic waves (CMW) in the holographic Weyl semimetal model	15
5.1	CMW in holographic WSM without Coulomb screening	15
5.2	CMW in holographic WSM with Coulomb screening	16
5.3	Properties of CMW and screened conductivity in holographic WSM	17
6	Conclusions	20
A	Equations of motion	23
A.1	Equations for the longitudinal fluctuations	23
A.2	Equations for the transverse fluctuations	24
A.3	On-shell action	25
B	Susceptibilities and conductivities	25
C	Coulomb screening, density-density correlation function and conductivities	27

1 Introduction

Even if a classical system was identical to its “mirror image”, its quantum counterpart would not be. This is the essence of the chiral anomaly which appears ubiquitously in all quantum many-body systems involving massless chiral fermions. The possibility of observing the quantum chiral anomaly at a macroscopic scale has stimulated various explorations and intellectual efforts in several physics research fields from high-energy to condensed matter [1, 2]. Dissipationless transport has been identified as one of the most promising routes in this regard, leading to the discovery of several anomaly-induced phenomena such as the chiral magnetic effect [3], the chiral separation effect [4] and the chiral vortical effect [5, 6]. In addition to these transport properties, the chiral anomaly also manifests itself at macroscopic scale in the low-energy dynamics by originating a novel propagating collective excitation known as the chiral magnetic wave (CMW) [7, 8]. The CMW represents a propagating wave

of fluctuating vector and axial charge densities that is expected to appear, as a result of the interplay between the chiral magnetic effect (CME) and the chiral separation effect (CSE), in chiral anomalous systems when exposed to a background magnetic field \vec{B} .

The experimental identification of propagating CMW in chiral anomalous systems is an active area of research [9–11]. In this chase, a prime candidate has always been the quark-gluon plasma (QGP), a highly energetic quantum soup of quarks and gluons generated in heavy ion collisions, as those produced in the relativistic heavy ion collider (RHIC) or large hadron collider (LHC). Numerical simulations have suggested that a gapless CMW would induce a chiral dipole moment, resulting in a possibly observable charge dependent elliptic flow in QGP [12]. The observation of a charge dependent elliptic flow has been reported in experiments [9–11, 13], seemingly supporting the existence of CMW in the QGP. Nevertheless, a thorough analysis indicated that it is impossible to definitively infer the existence of CMW from these experimental signatures [9–11]. This is attributed to the fact that the physical origin of the elliptic flow [9–11] cannot be exclusively ascribed to chiral anomalies, thereby complicating any conclusive statement [13, 14]. Additionally, from a theoretical perspective, it has been shown that, due to the relaxation of axial charge induced by dynamical gluonic fields and the screening effects associated with the dynamical electromagnetic field (Coulomb interactions), the propagating CMW becomes overdamped and remains therefore elusive to experimental observations [15–21]. In [17], it was concluded that because of these reasons, it is highly unlikely, if not even impossible, to detect an underdamped CMW in heavy ion collision experiments.

Topological semimetals, such as Dirac or Weyl semimetals (DSM or WSM), represent another important class of chiral anomalous systems [22]. Performing measurements on anomalous transport in such systems is certainly simpler compared to the complex QGP high-energy environment. In contrast to QGP, where the axial charge quickly relaxes due to not only the axial anomaly but also the contribution from the dynamical gluons [23], the axial charge in DSM or WSM could be nearly conserved, as suggested by the presence of a large negative magnetoresistance [24].

Additionally, in topological semimetals, the tunability of the dimensionless parameter eB/T^2 (with B the magnetic field, T the temperature and e the electric charge) potentially facilitates the observation of the chiral magnetic wave. Finally, the scattering time of Weyl fermions in topological semimetals spans a large range of values, from the long lifetime Weyl quasiparticle regime [25, 26] to the hydrodynamic strongly correlated one [27–29] and plasma regime [30]. All these factors together create favorable conditions that could potentially enable the observation of CMW in such anomalous systems. Therefore, a theoretical study of CMW in topological semimetals is timely and necessary to ascertain this further.

The objective of this study is to investigate the fate of CMW in a class of strongly coupled topological semimetals described by holography [31, 32], in which time reversal symmetry is broken while parity symmetry is preserved. In a weakly coupled WSM, due to the topological protection of the WSM phase, the system maintains its WSM characteristics even with an increasing separation of the Weyl nodes, provided that no topological phase transition occurs [32]. Consequently, as the distance between the Weyl nodes in the Brillouin zone increases, the transfer rate of chirality decreases, leading to an almost conserved axial

charge. It is natural to expect that similar physics occurs in the holographic counterpart, significantly influencing the dynamics of CMW as already anticipated in [15].

On top of that, Coulomb interactions are unavoidable in metals and semimetals [33–36], and they undoubtedly influence many of their properties such as the charge susceptibility and the electric conductivity [37]. The chiral magnetic wave, determined by the location of the lowest poles in the density-density correlation functions of electric and axial charge, is also subject to corrections due to Coulomb screening. In the holographic duality, the screening effect is attributed to the presence of a dynamical gauge field in the boundary system, achievable by using mixed-boundary conditions for the bulk gauge fields or equivalently the double-trace deformation (DTD) method [38–40]. This approach has been used in the literature in many instances, e.g., [41–48].

The focus of this work is to study the nature of the CMW, and the feasibility of its experimental observation, in strongly coupled Weyl semimetals by taking into account the effects of both axial charge relaxation and Coulomb interactions. More in general, our investigation aims to offer theoretical insights for potential experimental setups in table-top condensed matter systems.

This paper is organized as follows. In section 2, we construct the hydrodynamic theory for chiral magnetic waves with and without Coulomb interactions. In section 3, we review the holographic Weyl semimetal model and present the bulk solutions in the presence of a magnetic field in the probe limit. In section 4, we introduce Coulomb interactions in the holographic Weyl semimetals using mixed boundary conditions. In section 5, we investigate the dispersion relation of the collective chiral magnetic waves in strongly coupled Weyl semimetals by using the aforementioned holographic model. We conclude and discuss the most relevant open questions in section 6. The computational details and additional information can be found in appendices A to C.

2 Hydrodynamics of chiral magnetic waves in Dirac and Weyl semimetals

Chiral magnetic waves appear as a direct consequence of the combination of the chiral magnetic effect (CME) and the chiral separation effect (CSE) in the presence of a background magnetic field. As a result of these two effects, the vector charge ρ_V and the axial charge ρ_A are able to generate each other inducing the propagation of a pair of longitudinal waves — chiral magnetic waves. Aside from their longitudinal nature, this phenomenon is very similar to the propagation of electromagnetic waves created by the interplay between magnetic and electric fields and described by standard Maxwell equations. Recently, important analogies have been also found in comparison to the emergence of second sound in superfluids [49].

The chiral magnetic effect refers to the generation of a vector current along a background magnetic field direction B induced by a finite axial charge density [3], i.e.,

$$J_V^z = \sigma_{\text{CME}} B_z, \quad \sigma_{\text{CME}} = 8\alpha\mu_A, \quad (2.1)$$

where, without loss of generality, we choose the magnetic field along the z direction. Here, α is the chiral anomaly coefficient, σ_{CME} the chiral magnetic conductivity, and μ_A the axial chemical potential that relates to the axial charge density $\rho_A = \chi_A \mu_A$ via the corresponding

axial charge susceptibility χ_A . Similarly, the chiral separation effect is the generation of axial current along a background magnetic field direction B_z induced by a finite charge density, i.e.,

$$J_A^z = \sigma_{\text{CSE}} B_z, \quad \sigma_{\text{CSE}} = 8\alpha\mu_V, \quad (2.2)$$

where μ_V is the vector chemical potential. The vector charge density is then given by $\rho_V = \chi_V \mu_V$ with χ_V being the vector charge susceptibility.

The expressions mentioned above, and defining the CME and CSE, are valid only in the homogeneous case, where all quantities do not depend on the spatial coordinates. After introducing spatial dependence along the coordinate z , and taking into consideration dissipative dynamics, the constitutive equations for the vector and axial currents are given, to first order in derivatives $O(\partial)$ [8], by

$$\begin{aligned} J_V^z &= \sigma_{\text{CME}} B - \sigma_V \partial_z \mu_V = \frac{8\alpha B}{\chi_A} \rho_A - D_V \partial_z \rho_V, \\ J_A^z &= \sigma_{\text{CSE}} B - \sigma_A \partial_z \mu_A = \frac{8\alpha B}{\chi_V} \rho_V - D_A \partial_z \rho_A, \end{aligned} \quad (2.3)$$

where $B = B_z$. In the constitutive equations, eq. (2.3), we have assumed that parity symmetry is preserved and only time reversal symmetry is broken, to have the same symmetry pattern with the holographic Weyl semimetal set-up in section 3. σ_V, σ_A are respectively the vector and axial conductivities, and

$$D_V = \frac{\sigma_V}{\chi_V}, \quad D_A = \frac{\sigma_A}{\chi_A}, \quad (2.4)$$

are the diffusion constants for the vector and axial charges, respectively (Einstein relations). Moreover, in eq. (2.3) we have used the concrete expression for the CME and CSE conductivities from [3, 4]. Note that the susceptibilities $\chi_{A,V}$ and conductivities $\sigma_{A,V}$ in the constitutive equations eq. (2.3) are just one contribution to the total DC conductivities once axial charge relaxes over a long time scale introducing a Drude-like term, see appendix B. When the axial charge is conserved, the first order hydrodynamic transport coefficients in eq. (2.3) directly enter in the real part of the total DC conductivities.

In presence of a magnetic field \vec{B} along z direction, but in absence of an electric field \vec{E} , one has $\vec{E} \cdot \vec{B} = 0$ and the axial anomaly does not contribute to any dynamics. However, the U(1) axial symmetry is not a fundamental symmetry of nature; hence, axial charge is not a conserved quantity but it rather decays at a rate $\Gamma \equiv 1/\tau_5$. In Weyl semimetals, the axial charge relaxation time τ_5 is usually much larger than the quasi-particles lifetime [50]. Therefore, axial charge is approximately conserved. The dynamics are then governed by the conservation of the U(1) vector current and the softly broken non-conservation of the axial one [15],

$$\partial_\mu J_V^\mu = 0, \quad \partial_\mu J_A^\mu = -\Gamma \rho_A. \quad (2.5)$$

Here, the axial charge relaxation rate Γ is a phenomenological quantity that depends on temperature, magnetic field and the separation between the Weyl nodes. We notice that the second equation in eqs. (2.5) is meaningful only in the limit in which Γ is small (compared to the characteristic timescale of the system).

Combining the constitutive equations eqs. (2.3) with eqs. (2.5), we obtain the dispersion relations for the two lowest excitations

$$\omega_{\pm} = -\frac{i\Gamma}{2} - \frac{i}{2}(D_A + D_V)k_z^2 \pm \sqrt{\frac{(8\alpha B)^2}{\chi_A \chi_V} k_z^2 - \frac{((D_A - D_V)k_z^2 + \Gamma)^2}{4}}. \quad (2.6)$$

In the limit of small breaking of axial charge conservation, eventual corrections to σ_A, χ_A, D_A can be ignored, and one can consistently assume for simplicity that $\chi_A = \chi_V = \chi, \sigma_A = \sigma_V = \sigma$ and that all parameters only depend on B (see [8] for more details about the validity of this limit). Then, eq. (2.6) can be simplified to [15]

$$\omega_{\pm} = -\frac{i\Gamma}{2} - iDk_z^2 \pm \frac{1}{2}\sqrt{\frac{(16\alpha Bk_z)^2}{\chi^2} - \Gamma^2}. \quad (2.7)$$

The above dispersion relation indicates that, in presence of axial charge relaxation, chiral magnetic waves are not gapless propagating sound waves anymore. On the contrary, the real part of their dispersion is nonzero only above a critical wave-vector. This type of dispersion, gapped in momentum space, appears in several branches of physics [51]. As a concrete example, it is the dispersion expected for shear waves in classical liquids [52].

In addition to axial charge relaxation, in Dirac and Weyl semimetals, the inevitable Coulomb interactions play an important role as well. For example, at zero doping, Coulomb interactions can induce non-Fermi liquid behavior [33], and a further phase transition into an interaction-driven topological insulator [34, 35]. When we consider chiral magnetic waves, Coulomb interactions are also non-negligible. For example, the dielectric function gets screened by Coulomb effects [36]. The important effects of Coulomb interactions on chiral magnetic waves have been noticed and discussed for the first time in [17], casting serious doubts about the potential experimental detection of the latter in the quark-gluon plasma.

Simplifying the analysis by restricting it along the z direction, the parity-preserved longitudinal currents can be now written as

$$\begin{aligned} J_z^V &= \sigma_{\text{CME}} B + \sigma (E_z - \partial_z \mu_V) = \frac{8\alpha B}{\chi_A} \rho_A - D \partial_z \rho_V + \sigma E_z, \\ J_z^A &= \sigma_{\text{CSE}} B - \sigma \partial_z \mu_A = \frac{8\alpha B}{\chi_V} \rho_V - D \partial_z \rho_A \end{aligned} \quad (2.8)$$

where, as a consequence of dynamical electromagnetism, an electric field is naturally generated by the presence of charge. In particular, the electric field satisfies Gauss's law $\vec{\nabla} \cdot \vec{E} = \rho_V / \varepsilon_e$ where ε_e is the electric permittivity. Let us emphasize that, at this point, the electric field E_z is not external but rather a dynamical field. Eqs. (2.8) are the most general constitutive relations for the currents, since there are no Hall effect terms for the longitudinal currents in the probe limit, i.e., when we ignore the variations of the temperature δT and velocity δu^μ . Also, terms like $B \cdot \delta \sigma_{\text{CME}}$ and $B \cdot \delta \sigma_{\text{CSE}}$, that capture non-linear effects in the magnetic field, do not appear at this order. As shown below, in our setup, the dynamical magnetic field vanishes and, as a consequence, there are no terms like $\sigma_{\text{CME}} \delta B$ or $\sigma_{\text{CSE}} \delta B$ either.

The above analysis is consistent with Maxwell equations,

$$\vec{\nabla} \cdot \vec{E} = \frac{\rho_V}{\varepsilon_e},$$

$$\begin{aligned}
\vec{\nabla} \cdot \vec{B} &= 0, \\
\vec{\nabla} \times \vec{B} &= \mu_m \vec{J} + \varepsilon_e \mu_m \frac{\partial \vec{E}}{\partial t}, \\
\vec{\nabla} \times \vec{E} &= -\frac{\partial \vec{B}}{\partial t}
\end{aligned} \tag{2.9}$$

where μ_m is the magnetic permeability. In the presence of a charge density $\rho_V(t, z)$, a longitudinal electric field $E_z(t, z)$ is generated according to Gauss's law. Since $\vec{\nabla} \times \vec{E} = 0$, there is no time-dependent magnetic field generated by the dynamical electric field, and we have only an external background magnetic field B_z . Finally, $\vec{\nabla} \cdot \vec{B} = 0$ is trivially satisfied and Ampere's law reduces to $\vec{J} + \varepsilon_e \frac{\partial \vec{E}}{\partial t} = 0$. This equation is nothing but the relaxation of electric lines in the presence of charged matter, which corresponds to the explicit breaking of the electric 1-form global symmetry [53].

Because of the EM-generated dynamical electric field, the axial anomaly does not vanish anymore and the dynamical equations become

$$\partial_\mu J_V^\mu = 0, \quad \partial_\mu J_A^\mu = 8\alpha \vec{E} \cdot \vec{B} - \Gamma \rho_A. \tag{2.10}$$

The above equations, together with the constitutive equations, lead to the corresponding dispersion relation for chiral magnetic waves,

$$\omega_\pm = -\frac{i\Gamma}{2} - \frac{i\sigma}{2\varepsilon_e} - iDk_z^2 \pm \frac{\sqrt{4\varepsilon_e (8\alpha B)^2 (\chi + \varepsilon_e k_z^2) - (\sigma - \varepsilon_e \Gamma)^2 \chi^2}}{2\varepsilon_e \chi}. \tag{2.11}$$

Notice that the dispersion relation eq. (2.11) gets corrected by both axial relaxation and Coulomb screening effects, which is beyond the results of [8], where neither of these effects is included, and of [15] where only axial relaxation is considered.

Using a non-relativistic hydrodynamic framework for WSM, CMW along with other collective modes have been investigated in [29], where a steady state of the chiral electron fluid is realized by introducing momentum dissipation in the Euler equation. In contrast, our setup does not consider the dynamics of energy and momentum (which are not relevant for the holographic model in the probe limit) and Ohm's law appears directly in the constitutive equation for the dynamical electric field self-generated by the near-equilibrium Weyl plasma. Let us stress that the analysis in [29] is limited to the hydrodynamic framework where the hydrodynamic parameters cannot be determined. On the contrary, in our case we will make use of the holographic model as a microscopic description allowing a direct estimate of all the hydrodynamic coefficients as well.

The results in absence of Coulomb interactions presented above in eq. (2.7) can be obtained by sending $\varepsilon_e \rightarrow \infty$ in eq. (2.11). We remind that χ and σ here are the unscreened transport coefficients computed in absence of Coulomb interactions. Later on, we will discuss this point in more detail, and we will show that the dispersion relations in eqs. (2.11) are nothing but the poles of the screened current-current correlator.

3 Magnetic field effects on holographic Weyl semimetals

We consider the holographic Weyl semimetal model [31, 32] (see [54] for a review) described by the five-dimensional bulk action

$$S = \int d^5x \sqrt{-g} \left[\frac{1}{2\kappa^2} \left(R + \frac{12}{L^2} \right) - \frac{1}{4e^2} \mathcal{F}^2 - \frac{1}{4e^2} F^2 - (D_\mu \Phi)^* (D^\mu \Phi) - V(\Phi) \right. \\ \left. + \epsilon^{\mu\nu\rho\sigma\tau} A_\mu \left(\frac{\alpha}{3} (F_{\nu\rho} F_{\sigma\tau} + 3\mathcal{F}_{\nu\rho} \mathcal{F}_{\sigma\tau}) \right) \right], \quad (3.1)$$

with $\mathcal{F}_{\mu\nu} = \partial_\mu V_\nu - \partial_\nu V_\mu$, $F_{\mu\nu} = \partial_\mu A_\nu - \partial_\nu A_\mu$ and $D_\mu \Phi = (\partial_\mu - iqA_\mu)\Phi$. The axial anomaly in the dual field theory is introduced using Chern-Simons terms proportional to α that are determined by the anomalous structure of the currents. The ratio between the coefficients of $A \wedge F \wedge F$ and $A \wedge \mathcal{F} \wedge \mathcal{F}$ is fixed by considering the consistent current choice where the vector current is conserved and only the conservation of axial current is broken (by anomaly).¹ The complex scalar field Φ couples to the axial vector field A_μ and its scalar potential is given by $V(\Phi) = m^2 |\Phi|^2$. Whenever this scalar has a non-zero boundary source, axial symmetry is explicitly broken and axial charge relaxes. Here, we choose the scalar mass $m^2 = -3$ and switch on only the z component of the axial gauge field A_z . Without loss of generality, we will choose $2\kappa^2 = L^2 = e^2 = 1$ in the rest of the manuscript.

With these definitions, the consistent currents in the dual field theory can be defined by the following expressions [2]

$$J_V^\mu = \lim_{r \rightarrow \infty} \frac{\delta S}{\delta V_\mu} = \lim_{r \rightarrow \infty} \sqrt{-g} (\mathcal{F}^{\mu r} + 4\alpha \epsilon^{r\mu\nu\rho\sigma} A_\nu \mathcal{F}_{\rho\sigma}), \quad (3.2)$$

$$J_A^\mu = \lim_{r \rightarrow \infty} \frac{\delta S}{\delta A_\mu} = \lim_{r \rightarrow \infty} \sqrt{-g} \left(F^{\mu r} + \frac{4}{3} \alpha \epsilon^{r\mu\nu\rho\sigma} A_\nu F_{\rho\sigma} \right), \quad (3.3)$$

where r is the radial coordinate in the bulk and $r = \infty$ is the UV AdS boundary.

The Ward identities for the consistent currents are then

$$\partial_\mu J_V^\mu = 0, \\ \partial_\mu J_A^\mu = \lim_{r \rightarrow \infty} \sqrt{-g} \left(-\frac{\alpha}{3} \epsilon^{r\mu\nu\rho\sigma} (F_{\mu\nu} F_{\rho\sigma} + 3\mathcal{F}_{\mu\nu} \mathcal{F}_{\rho\sigma}) - iq[\Phi(D^r \Phi)^* - \Phi^*(D^r \Phi)] \right) + \text{c.t.}, \quad (3.4)$$

where ‘‘c.t.’’ stands for contact terms. As expected, the vector current is conserved. On the contrary, the axial current is not conserved due to the axial anomaly proportional to α and the effects of the scalar field Φ . When $\vec{E} = 0$, $\vec{B} \neq 0$, only a source for the scalar field can explicitly break axial charge conservation.

3.1 The solution in the probe limit

We work in the probe limit in the presence of background magnetic field and at finite temperature. In the context of holographic Weyl semimetals, the probe limit is a reasonable approximation as long as the system is not too close to the quantum critical point and B_z is not parametrically larger than temperature [55].

¹We use the following convention for Levi-Civita symbol $\tilde{\epsilon}_{txyzr} = 1$ or $\tilde{\epsilon}^{txyzr} = -1$, and the Levi-Civita tensor $\epsilon_{\mu\nu\rho\sigma\tau} \equiv \sqrt{-g} \tilde{\epsilon}_{\mu\nu\rho\sigma\tau}$ and $\epsilon^{\mu\nu\rho\sigma\tau} \equiv \frac{1}{\sqrt{-g}} \tilde{\epsilon}^{\mu\nu\rho\sigma\tau}$.

In order to study chiral magnetic waves in WSM, we consider the simplest setup with

$$\mu = \mu_5 = \rho_5 = 0, \quad \rho \neq 0, \quad \vec{E} = 0, \quad B_z \neq 0, \quad b_z \neq 0, \quad M \neq 0. \quad (3.5)$$

From the bulk point of view, this corresponds to the AdS-Schwarzschild solution where we neglect the backreaction of matter field on the metric, i.e.,

$$ds^2 = -udt^2 + \frac{dr^2}{u} + r^2 d\vec{x}^2, \quad u(r) = r^2 \left(1 - \frac{r_h^4}{r^4}\right), \quad (3.6)$$

$$V = V_t dt + \frac{B}{2}(ydx - xdy), \quad A = A_z dz, \quad \Phi = \phi(r).$$

Here $B = B_z$ is in the same direction of z .

The asymptotic behaviors of the matter fields near to the AdS boundary, $r \rightarrow \infty$, are given by

$$\begin{aligned} r\phi(r) &= M + \dots, \\ A_z(r) &= b + \dots, \\ V_t(r) &= \mu + \dots \end{aligned} \quad (3.7)$$

where M corresponds to a source for the dual scalar operator that breaks U(1) axial symmetry, b relates to the separation of the chiral nodes and μ is the chemical potential in the boundary field theory. We will be interested in zero chemical potential states.

The equations of motion for A_z , ϕ , and V_t are

$$\begin{aligned} A_z'' + \left(\frac{1}{r} + \frac{u'}{u}\right) A_z' - \frac{2q^2\phi^2}{u} A_z + \frac{8\alpha B}{ru} V_t' &= 0, \\ \phi'' + \left(\frac{3}{r} + \frac{u'}{u}\right) \phi' - \left(\frac{m^2}{u} + \frac{q^2 A_z^2}{r^2 u} + \frac{\lambda\phi^2}{u}\right) \phi &= 0, \\ V_t'' + \frac{3}{r} V_t' + \frac{8\alpha B}{r^3} A_z' &= 0. \end{aligned} \quad (3.8)$$

Notice that the last equation in (3.8) reduces to a total derivative

$$(r^3 V_t' + 8\alpha B A_z)' = 0, \quad (3.9)$$

and its solution can be formally written as

$$V_t(r) = \int_{r_0}^r \frac{ds}{s^3} (c_1 - 8\alpha B A_z(s)) + c_2, \quad (3.10)$$

where c_1 and c_2 are integration constants. As required by the regularity conditions, V_t vanishes at the horizon, i.e., $c_2 = 0$. The choice of c_1 is arbitrary and is related to the chemical potential μ in the field theory. We will focus on zero chemical potential states $\mu = 0$ via choosing c_1 that is a function of the parameters in the boundary field theory.

For later convenience, we define the dimensionless parameters in our system as

$$\tilde{B} \equiv \frac{B}{\pi^2 T^2}, \quad \tilde{M} \equiv \frac{M}{\pi T}, \quad \tilde{b} \equiv \frac{b}{\pi T}. \quad (3.11)$$

3.2 Magnetic field effects on the phase diagram

An interesting question arises when we switch on a magnetic field in a Weyl semimetal, that is, does the topological phase still exist or is it broken by the magnetic field? In other words, does the magnetic field change the phase diagram and the topological phase transition between a topological Weyl semimetal to a gapped trivial phase?

In the weakly coupled field theory [56, 57], this can be investigated by solving the Landau levels from the Hamiltonian where the electrons couple to the magnetic field B . One can find [56, 57] that the chiral conduction band splits into an infinite number of Landau levels in the presence of B . Importantly, the lowest Landau level remains the chiral band and it is unchanged by B . More precisely, via tuning the ratio M/b between the mass and the time-reversal breaking in the Lorentz violating Dirac equation [58]

$$\left[\gamma^\mu (i\partial_\mu - eV_\mu) - \gamma^5 \gamma^z b - M \right] \Psi = 0 \quad (3.12)$$

in the presence of the magnetic field, $V_\mu = (0, By/2, -Bx/2, 0)$, the topological phase transition pattern remains unchanged. Now, the energy spectrum is made of Landau Levels. The lowest one is defined by the dispersion

$$E_0 = b \pm \sqrt{k_z^2 + M^2}, \quad (3.13)$$

where we have set $k_x = k_y = 0$. Expression (3.13) takes exactly the same form as without magnetic field. The detailed expression for higher Landau levels can be found in e.g. [57]. The key observation is that the magnetic field does not alter the lowest band structure. However, this analysis is reliable only when the magnetic field is sufficiently small, since otherwise the degrees of freedom from the higher Landau levels would get excited as well, spoiling this approximation.

In strongly coupled Weyl semimetals, the notion of electronic bands is absent and the anomalous Hall conductivity (AHE) serves as the order parameter to identify the Weyl semimetal phase and the topological phase transition [31, 32]. To compute the AHE, the transverse sector of fluctuations at $k_z = 0$ is switched on, i.e., $\delta v_x, \delta v_y, \delta a_x, \delta a_y$. The EOMs for the transverse sector are summarized in appendix A.2. It turns out that in the probe limit with background magnetic field the holographic formula for the anomalous Hall effect remains unchanged,

$$\sigma_{\text{AHE}} = 8\alpha A_z(r_h), \quad (3.14)$$

and depends only on the horizon behavior of A_z .

The structure of the phase diagram for different values of the magnetic field B can be obtained by looking at the order parameter σ_{AHE} shown in figure 1. For small magnetic field, for which the probe limit is valid,² the inflection point does not move. Hence, the location of the quantum critical point in terms of the dimensionless parameter M/b does not depend on B (or on the sign of B). Interestingly, this phenomenon is the exactly same as in the weakly coupled theory in which the Weyl semimetal phase and the topological phase transition are dominated by the lowest Landau level that is independent of B .

²The backreaction of the magnetic field might have nontrivial effects on magnetotransport properties, e.g., [59].

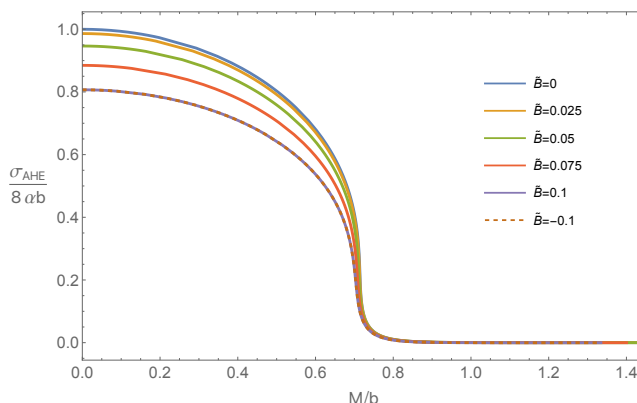


Figure 1. Anomalous Hall conductivity σ_{AHE} as a function of M/b for different, and small values of the dimensionless magnetic field \tilde{B} , at a low temperature $T/b = 1/(8\pi)$.

In the backreacted case with finite magnetic field, we do not have such a simple expression for AHE as eq. (3.14). This can be seen as follows. First, let us notice that there exists a topological Chern-Simons charge induced by the anomaly, i.e., $\rho_{\text{CS}} \propto \vec{b} \cdot \vec{B}$. In the gravitation theory, this indicates the necessity of having a nonzero time component of the vector gauge field $V_t \neq 0$. When we switch on the fluctuations to compute anomalous Hall conductivity, this non-vanishing potential couples the fluctuations of vector and metric fields together, making the computations complicated. In this case the anisotropy of the butterfly velocity has been investigated as an effective probe of the phase transition [57]. In this work, we focus on the probe limit for simplicity.

3.3 Axial charge relaxation time

When axial charge conservation is weakly broken, the conservation equation is modified into

$$\partial_\mu J_A^\mu = -\Gamma \rho_A, \tag{3.15}$$

which indicates that the axial charge ρ_A decays with a relaxation time $\tau_5 \equiv 1/\Gamma$. This relaxation time τ_5 can be computed by looking at the corresponding purely imaginary pole in the axial charge density-density correlation function of, i.e.,

$$\tau_5^{-1} \equiv -\text{Im}(\omega^*) = \Gamma, \tag{3.16}$$

where ω^* is the non-hydrodynamic pole related to axial charge relaxation. In the holographic dual picture, the pole in the correlation function can be derived from the quasi-normal modes (QNM) spectrum of the bulk theory.

The dependence of the axial relaxation time τ_5 on \tilde{b} is shown in the left panel of figure 2. The horizontal axis represents the dimensionless separation of the Weyl nodes in wave-vector space, \tilde{b} , while the vertical axis represents the inverse axial charge relaxation time normalized by temperature, $(\tau_5 T)^{-1}$. We observe that $(\tau_5 T)^{-1}$ decreases monotonically by increasing \tilde{b} for all values of \tilde{M} . In the small \tilde{b} regime, we find that the decay can be well approximated by a quadratic power law scaling. In the large \tilde{b} regime, τ_5^{-1} decays to zero. This indicates that even in the small external magnetic field regime, $B \ll T^2$, with fixed \tilde{M} , $\tau_5 T$ can be made

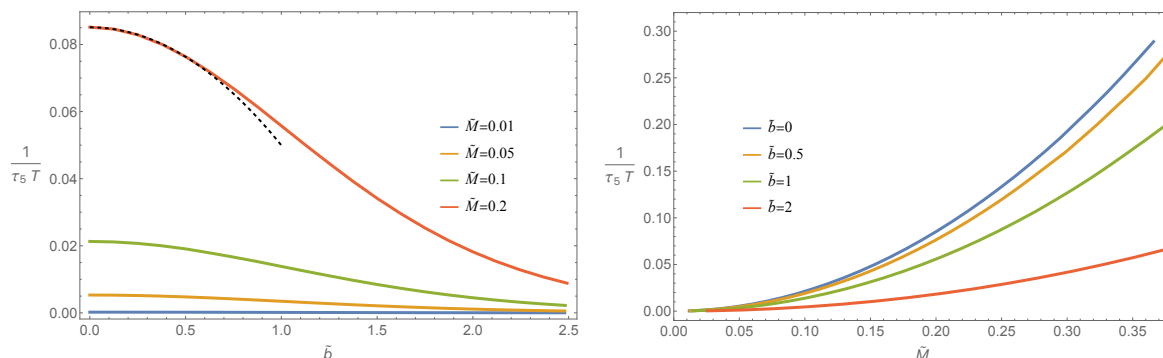


Figure 2. *Left:* the dimensionless axial relaxation time as a function of \tilde{b} for different values of \tilde{M} with fixed $\tilde{B} = 0.1$. In the small \tilde{b} regime, the decrease in $(\tau_5 T)^{-1}$ obeys a square law in terms of \tilde{b} which is shown by the dashed black curve. *Right:* $(\tau_5 T)^{-1}$ as a function of \tilde{M} , for different values of \tilde{b} .

arbitrarily large by taking the limit $M/b \rightarrow 0$. This is consistent with the physical intuition that the larger the distance between the two chiral nodes in the Brillouin zone, the more inhibited the processes between the two nodes that do not conserve chirality. For completeness, we show the dependence of $(\tau_5 T)^{-1}$ on \tilde{M} for different \tilde{b} in the right panel of figure 2. The results are consistent and show that the axial relaxation rate Γ follows approximately a quadratic power law behavior $\Gamma \simeq a\tilde{M}^2$ where the coefficient a decreases as we increase \tilde{b} .

Interestingly, the axial relaxation time τ_5 displays a universal relation

$$(\tau_5 T)^{-1} \simeq \frac{2}{\chi_A} \phi_h^2, \tag{3.17}$$

where $\phi_h \equiv \phi(r_h)$ is the horizon value of the bulk scalar field. The coefficient $2/\chi_A$ depends only on the magnetic field B and not on \tilde{b} , as demonstrated in the right panel of figure 3. This relation indicates that τ_5 , or equivalently Γ , depends only on a single IR quantity ϕ_h . Nevertheless, it is important to notice that such an horizon value does not have a clear interpretation from the boundary field theory perspective, where it is a function of both \tilde{M} and \tilde{b} . This universal relation is robust against variations of temperature T , magnetic field B , the chiral separation b , and the fermion mass M .

Eq. (3.17) can be obtained as follows. In holography, the longitudinal DC conductivity in the presence of a background magnetic field B and axial relaxation reads

$$\sigma_{\text{DC}} = \pi T + \frac{32B^2\alpha^2}{\pi^3 T^3 q^2 \phi_h^2}, \tag{3.18}$$

where the second term is proportional to B^2 due to the axial charge relaxation and represents the phenomenon of negative magnetoresistance [27, 55]. On the other hand, the longitudinal DC conductivity can also be calculated from chiral hydrodynamics [27] at zero densities,

$$\sigma_{\text{DC}} = \sigma_V + \frac{(8B\alpha)^2 \tau_5}{\chi_A}, \tag{3.19}$$

where $\sigma_V \simeq \pi T$ since the above formulae are valid only when the magnetic field is weak and the axial relation time is long.

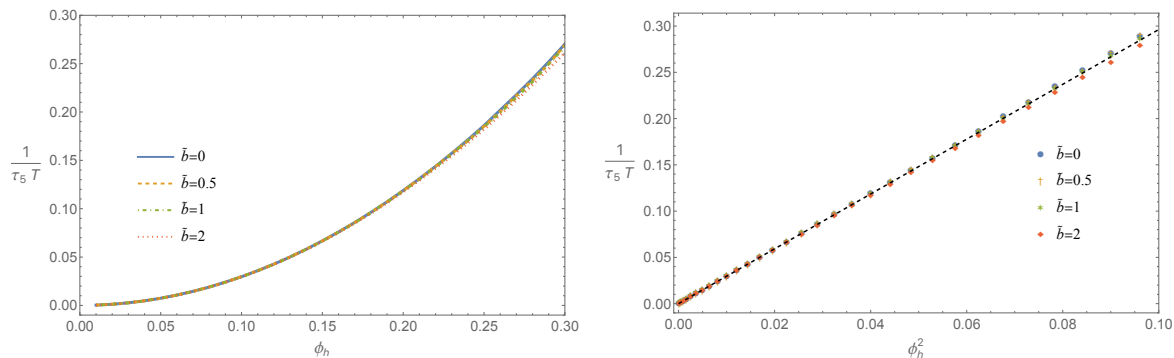


Figure 3. The universal relation between Γ and the horizon value of the bulk scalar field, i.e. $\phi_h \equiv \phi(r_h)$. In the right panel, a different representation which emphasizes the universal behavior $\tau_5^{-1} \simeq \frac{2}{\chi_A} \phi_h^2$ (dashed black line) where χ_A only depends on B .

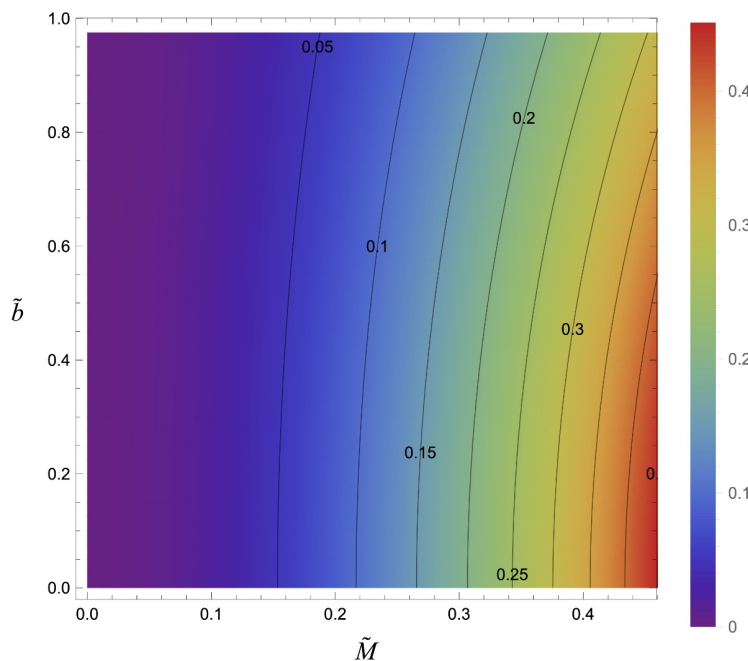


Figure 4. Contour plot of $(\tau_5 T)^{-1}$ in the \tilde{M} - \tilde{b} plane for $\tilde{B} = 0.1$.

Comparing the two equations, eq. (3.18) and eq. (3.19), we conclude that

$$\Gamma = \tau_5^{-1} \simeq 2\pi^3 T^3 \frac{q^2 \phi_h^2}{\chi_A}, \tag{3.20}$$

which is exactly the universal relation found numerically in figure 3 where we work in the unit $\pi T = 1$ and have set $q = 1$. Note that this relation is valid only when $B/T^2 \ll 1$ and $\tau_5 T \ll 1$.

To summarize our findings, we present a contour plot of $(\tau_5 T)^{-1}$ in the \tilde{M} - \tilde{b} plane in figure 4. The changes in the rainbow color confirm that $(\tau_5 T)^{-1}$ increases with \tilde{M} , and the more and more dense contour lines indicate the quadratic increase. Finally, the vertical bending in the contour lines shows that chiral separation increases the lifetime of axial charge.

4 Coulomb interactions in the holographic Weyl semimetal model

Coulomb interactions are inevitably present in Dirac and Weyl semimetals, and impose corrections to the transport properties. As a concrete example, the susceptibility is defined from the second order variation of the free energy with respect to the charge density. Coulomb interactions between electrons and ions contribute to the free energy and hence the susceptibility gets screened.

In the presence of Coulomb interactions, the dynamical density-density correlation function in the random-phase approximation (RPA) is (see appendix C for details)

$$\chi_{\text{sc}}(\omega, \vec{k}) = \frac{\chi(\omega, \vec{k})}{1 - \frac{\lambda_e}{|\vec{k}|^2} \chi(\omega, \vec{k})}, \quad (4.1)$$

where the inverse momentum squared indicates the Coulomb potential in the momentum representation. λ_e is the electromagnetic coupling constant, which is left as a tunable parameter. On the left side, $\chi_{\text{sc}}(\omega, \vec{k})$ is the screened density-density correlation function in response to the external charge density ρ_{ext} . On the right side, $\chi(\omega, \vec{k})$ is the unscreened density-density correlation in response to the external gauge potential v_{ext} that dictates the response of the system in absence of the Coulomb potential.

Coulomb interactions have also important effects on the electric conductivity. In their presence, the (locally resolved) screened longitudinal conductivity σ_{sc} is given in terms of the unscreened one σ as

$$\sigma_{\text{sc}}(\omega, \vec{k}) = \frac{\sigma(\omega, \vec{k})}{1 - \frac{\lambda_e}{i\omega} \sigma(\omega, \vec{k})}, \quad (4.2)$$

which is also based on RPA.

Coulomb interactions lead to different poles in the screened density-density and current-current correlation functions with respect to their unscreened counterparts. The ratio between the unscreened susceptibility (conductivity) and the screened susceptibility (conductivity) defines the dynamical dielectric function, i.e.,

$$\epsilon(\omega, \vec{k}) \equiv 1 - \frac{\lambda_e}{|\vec{k}|^2} \chi(\omega, \vec{k}) = 1 - \frac{\lambda_e}{i\omega} \sigma(\omega, \vec{k}), \quad (4.3)$$

which plays a fundamental role in this discussion and which reduces to 1 in absence of Coulomb interactions. We can now anticipate the different meanings of poles of $\chi(\omega, \vec{k})$ and $\chi_{\text{sc}}(\omega, \vec{k})$ and their interpretation in the holographic side. To compute the poles of $\chi(\omega, \vec{k})$, we must take Dirichlet boundary conditions for the vector gauge field at the boundary. This means that we switch off the external source of the charge density, e.g., $v_{\text{ext}} = 0$. On the contrary, to compute the poles of $\chi_{\text{sc}}(\omega, \vec{k})$, we take the dynamical dielectric function to vanish

$$\epsilon(\omega, \vec{k}) = 0, \quad (4.4)$$

which corresponds to the external charge density ρ_{ext} to vanish, i.e., $\rho_{\text{ext}} = 0$. In the zero wave-vector limit $\vec{k} \rightarrow 0$, $\epsilon(\omega = \Omega_{\text{pl}}, \vec{k} \rightarrow 0) = 0$ gives the plasma frequency $\omega = \Omega_{\text{pl}}$. We refer to [60] for a nice discussion on this point in holography.

Here, we consider a dynamical gauge field in the boundary field theory by imposing mixed boundary conditions for the vector gauge field. We start from the total action for the gauge field

$$S_{\text{total}}^V = \int d^5x \sqrt{-g} \left[-\frac{1}{4} \mathcal{F}^2 + \alpha \epsilon^{\mu\nu\rho\sigma\tau} A_\mu \mathcal{F}_{\nu\rho} \mathcal{F}_{\sigma\tau} \right] + \int_{r=r_\infty} d^4x \sqrt{-\gamma} \left[\frac{\log r}{4} \mathcal{F}^2 - \frac{1}{4\lambda_e} \mathcal{F}^2 + V_\mu J_{\text{ext}}^\mu \right], \quad (4.5)$$

where the last two terms are a boundary kinetic term and a Legendre transform. Then, S_{total}^V leads to the equation of motion

$$\Pi_V^\mu - \frac{1}{\lambda_e} \partial_\nu \mathcal{F}^{\mu\nu} + J_{\text{ext}}^\mu = 0, \quad (4.6)$$

where λ_e is the electromagnetic coupling at the boundary since we have fixed the bulk electromagnetic coupling to unit in the bulk. Considering the time component of eq. (4.6), we find the electric permittivity (by comparing with eq. (2.9))

$$\varepsilon_e = 1/\lambda_e. \quad (4.7)$$

The conjugate momentum Π_V^μ along the radial direction is given by

$$\Pi_V^\mu = \lim_{r \rightarrow \infty} \frac{\delta S_{\text{ren}}}{\delta V_\mu} = \lim_{r \rightarrow \infty} \sqrt{-g} (\mathcal{F}^{\mu r} + 4\alpha \epsilon^{r\mu\nu\rho\sigma} A_\nu \mathcal{F}_{\rho\sigma}). \quad (4.8)$$

Here, we have taken the saddle point approximation and S_{ren} is the renormalized on-shell action defined in eq. (A.14). The radial conjugate momentum corresponds to the U(1) vector current $\Pi_V^\mu = J_V^\mu$ with $\partial_\mu \Pi_V^\mu = 0$ such that eq. (4.8) is simply the Maxwell equation in the boundary field theory.

In terms of the boundary expansions ($r \rightarrow \infty$)

$$\begin{aligned} v_t &= v_t^{(0)} + \frac{v_t^{(1)}}{r^2} \log r - \frac{v_t^{(2)}}{r^2} + \dots, & v_z &= v_z^{(0)} + \frac{v_z^{(1)}}{r^2} \log r + \frac{v_z^{(2)}}{r^2} + \dots, \\ a_t &= a_t^{(0)} + \frac{a_t^{(1)}}{r^2} \log r - \frac{a_t^{(2)}}{r^2} + \dots, & a_z &= a_z^{(0)} + \frac{a_z^{(1)}}{r^2} \log r + \frac{a_z^{(2)}}{r^2} + \dots, \end{aligned} \quad (4.9)$$

we have

$$\begin{aligned} \Pi_V^t &= 2v_t^{(2)} + 8\alpha B a_z^{(0)}, & \partial_\mu \mathcal{F}^{\mu t} &= k_z (\omega v_z^{(0)} + k_z v_t^{(0)}), \\ \Pi_V^z &= 2v_z^{(2)} - 8\alpha B a_t^{(0)}, & \partial_\mu \mathcal{F}^{\mu z} &= \omega (\omega v_z^{(0)} + k_z v_t^{(0)}). \end{aligned} \quad (4.10)$$

The first-order variation of the conjugate momentum immediately follows as

$$\begin{aligned} \delta \Pi_V^t &= 2 \delta v_t^{(2)} + 8\alpha B \delta a_z^{(0)}, & \delta \left(\frac{1}{\lambda_e} \partial_\mu \mathcal{F}^{\mu t} \right) &= \frac{k_z}{\lambda_e} \left(\omega \delta v_z^{(0)} + k_z \delta v_t^{(0)} \right), \\ \delta \Pi_V^z &= 2 \delta v_z^{(2)} - 8\alpha B \delta a_t^{(0)}, & \delta \left(\frac{1}{\lambda_e} \partial_\mu \mathcal{F}^{\mu z} \right) &= \frac{\omega}{\lambda_e} \left(\omega \delta v_z^{(0)} + k_z \delta v_t^{(0)} \right), \end{aligned} \quad (4.11)$$

and therefore

$$\begin{aligned} \delta J_{\text{ext}}^t &= -2 \delta v_t^{(2)} - 8\alpha B \delta a_z^{(0)} - \frac{k_z}{\lambda_e} \left(\omega \delta v_z^{(0)} + k_z \delta v_t^{(0)} \right), \\ \delta J_{\text{ext}}^z &= -2 \delta v_z^{(2)} + 8\alpha B \delta a_t^{(0)} - \frac{\omega}{\lambda_e} \left(\omega \delta v_z^{(0)} + k_z \delta v_t^{(0)} \right). \end{aligned} \quad (4.12)$$

In terms of the U(1) gauge invariant quantity $v \equiv v_t + \frac{\omega}{k_z} v_z$, we obtain the variation rule

$$\begin{aligned} \delta J_{\text{ext}}^t &= -\frac{2k_z^2}{\omega^2 - k_z^2} \delta v^{(2)} - 8\alpha B \delta a_z^{(0)} - \frac{k_z^2}{\lambda_e} \delta v^{(0)}, \\ \delta J_{\text{ext}}^z &= -\frac{2\omega k_z}{\omega^2 - k_z^2} \delta v^{(2)} + 8\alpha B \delta a_t^{(0)} - \frac{\omega k_z}{\lambda_e} \delta v^{(0)}. \end{aligned} \tag{4.13}$$

Setting the external currents above to zero corresponds to a vanishing dynamical dielectric function, and gives us therefore the poles of the screened density-density correlation function.

5 Chiral magnetic waves (CMW) in the holographic Weyl semimetal model

Let us first briefly review some general properties of the chiral magnetic waves. Since CMW appear both for finite densities $\mu \neq 0, \mu_5 \neq 0$ and zero densities $\mu = \mu_5 = 0$, for simplicity, we limit our analysis to the second simpler case.

In the absence of a magnetic field and axial charge relaxation, i.e., $B = \Gamma = 0$, both the vector and axial charges diffuse at late time, corresponding to two independent hydrodynamic diffusive modes. Switching on a background magnetic field, $B \neq 0, \Gamma = 0$, due to the axial anomaly, the two diffusive modes mix with each other via the CME and CSE and result in two propagating modes — chiral magnetic waves [8]. Instead, by switching off the magnetic field and considering the axial charge relaxation effect, i.e. $B = 0, \Gamma \neq 0$, the axial charge diffusive mode becomes a non-hydrodynamic gapped diffusive mode (described by a U(1) quasi-hydrodynamic theory [61]) while the diffusive mode corresponding to vector charge fluctuations remains unchanged.

In the presence of both the magnetic field and axial charge relaxation, i.e. $B \neq 0, \Gamma \neq 0$, the diffusive hydrodynamic mode arising from the conservation of the vector charge and the gapped non-hydro mode induced from the non-conserved axial charge display a complex interplay. This situation has been studied numerically in [15] but without considering the separation between the Weyl nodes which is relevant for the case of WSM.

5.1 CMW in holographic WSM without Coulomb screening

We first consider the simplest case without Coulomb screening. With the help of numerical techniques, we demonstrate that the dispersion relation of CMWs in holographic WSM is in perfect agreement with the predictions in eq. (2.7) from chiral quasi-hydrodynamics. We provide an example in figure 5, where the orange solid lines represent the analytical predictions from eq. (2.7), while the blue dots are the numerical results from the holographic computations. We have checked that as long as $\tau_5 T \gg 1$, eq. (2.7) fits well the numerical results.

The spectrum displays a hydrodynamic diffusive mode and a non-hydrodynamic transient mode that collide on the imaginary axes at a real value of the wave-vector k_c . Above such a value a real part of the dispersion develops and for $k \gg k_c$ a propagating wave re-emerges. Following (2.7), the location of the critical point is given by

$$k_c = \frac{\Gamma\chi}{16\alpha B}, \quad \omega_c = -\frac{i\Gamma}{2} - iD \left(\frac{\Gamma\chi}{16\alpha B} \right)^2, \tag{5.1}$$

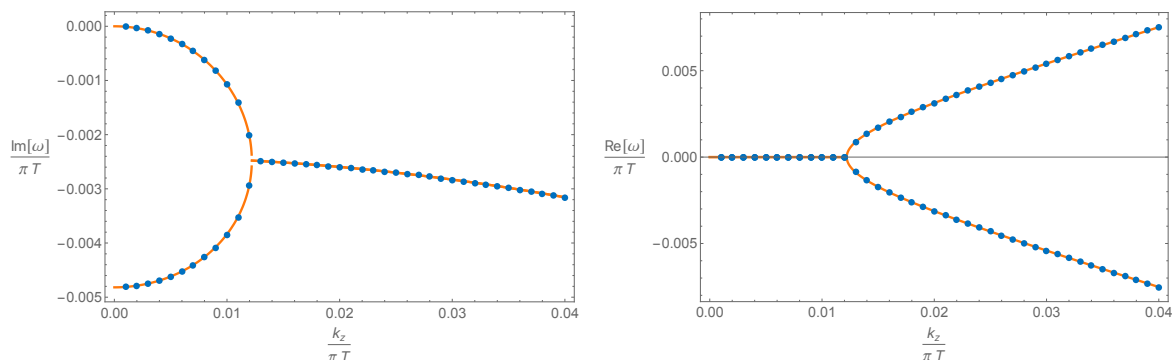


Figure 5. The two lowest QNMs with $\tilde{B} = 0.05$, $\tilde{b} = 1$, $M/b = 0.1$. The numerical results are shown by the numerical points while the prediction from quasi-hydrodynamics in eq. (2.7) by the solid lines.

in the slow axial relaxation regime $\tau_5 T \gg 1$. Here, χ and D are only functions of B . When we fix B, M and T , Γ decreases monotonically with respect to chiral separation parameter b , as shown in figure 2. As a consequence, chiral separation decreases the value of the critical wave-vector k_c pushing the propagating regime towards smaller wave-vectors.

5.2 CMW in holographic WSM with Coulomb screening

Next, we take Coulomb interactions into consideration as a more realistic scenario for conducting semimetals. We recall the corresponding dispersion relation for the lowest excitations

$$\omega_{\pm} = -\frac{i\Gamma}{2} - \frac{i\sigma}{2\varepsilon_e} - iDk_z^2 \pm \frac{\sqrt{4\varepsilon_e(8\alpha B)^2(\chi + \varepsilon_e k_z^2) - (\sigma - \varepsilon_e \Gamma)^2 \chi^2}}{2\varepsilon_e \chi}. \quad (5.2)$$

One can notice that there are two timescales that might possibly destroy the hydrodynamic nature of the modes in eq. (5.2): (I) $\tau_5^{-1} = \Gamma$ that comes from axial relaxation and (II) $\tau^{-1} = \sigma/\varepsilon_e$ that arises because of electric field relaxation due to Coulomb screening. Let us first assume $\tau_5 \gg \tau$ so that axial relaxation can be ignored, i.e. $\Gamma = 0$. Then, we have

$$\omega_{\pm} = -\frac{i\sigma}{2\varepsilon_e} - iDk_z^2 \pm \frac{\sqrt{4\varepsilon_e(8\alpha B)^2(\chi + \varepsilon_e k_z^2) - \sigma^2 \chi^2}}{2\varepsilon_e \chi}. \quad (5.3)$$

This equation is quite interesting. By tuning the magnetic field B or the permittivity ε_e , the term in the square root can either be negative or positive as $k_z \rightarrow 0$, which is different from eq. (2.7), where that is always negative at $k_z = 0$.

When the term inside the square root is negative, the two modes are purely imaginary in the small momentum regime, which is similar to eq. (2.7). However, now both of ω_{\pm} have an imaginary gap since even the vector charge dissipates at long wavelength due to screening effects. This structure of the modes is very similar to what found in the linear axion model for momentum relaxation [62, 63]. It has also been found and discussed in the context of holographic plasmons [64–67], where nevertheless the dynamics are more complicated since they are a result of a three modes interaction. As an example, taking a sufficiently small B , figure 6 demonstrates this qualitative difference in comparison with figure 5. Notice that in this regime the gap is still in wave-vector space and there is no finite real part below k_c .

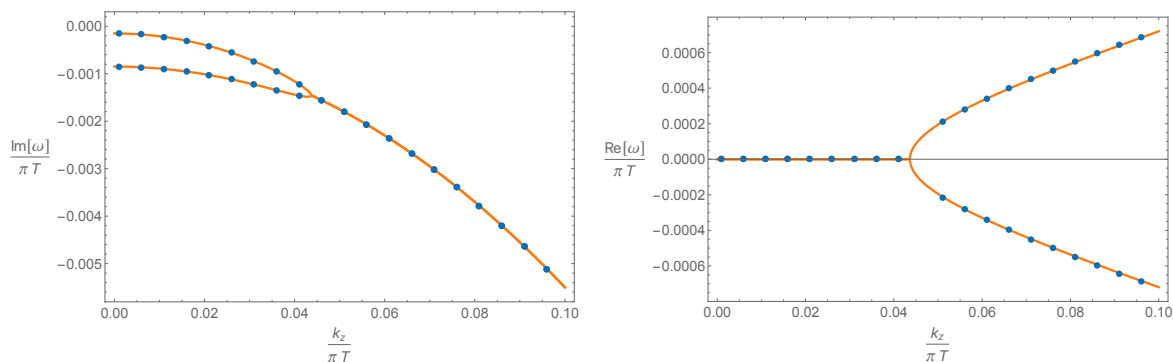


Figure 6. Lowest modes with $\tilde{B} = 0.002$, $\tilde{M} = \tilde{b} = 0$ and $\lambda_e/(\pi T) = 10^{-3}$. The numerical results are displayed by the numerical bullets while the quasi-hydrodynamical prediction from eq. (5.3) by solid lines.

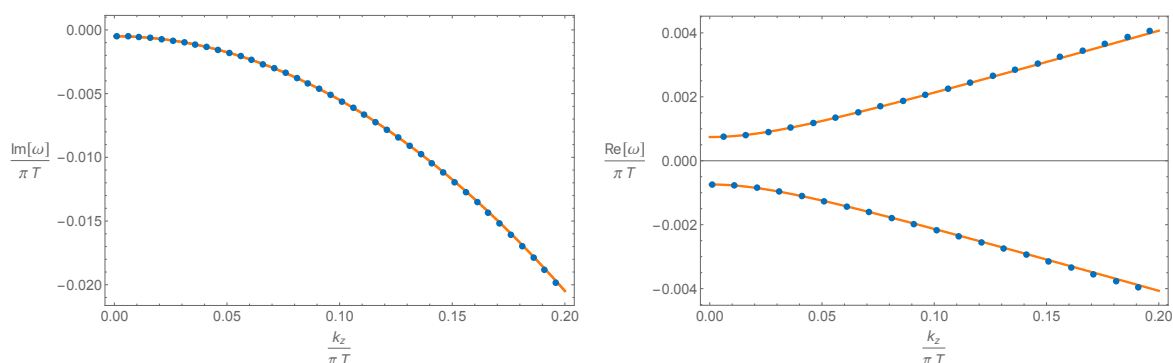


Figure 7. Lowest modes with $\tilde{B} = 0.005$, $\tilde{M} = \tilde{b} = 0$ and $\lambda_e/(\pi T) = 10^{-3}$. The numerical results are displayed by the numerical bullets while the quasi-hydrodynamical prediction from eq. (5.3) by solid lines.

As the magnetic field B increases and becomes larger than a critical value, the term in the square root in eq. (5.3) can become positive for arbitrary values of the wave-vector k . As a result, the critical momentum k_c does not exist anymore and the gap is transferred in frequency — a mass gap. Once again, notice the similarities with [63] (figure 10 therein). This implies the emergence of a mass/frequency gap in as illustrated in figure 7.

Now, let us move beyond the limit in which axial relaxation is negligible and consider $\Gamma \neq 0$. As Γ increases, the real parts in ω_{\pm} are suppressed. Reaching a critical Γ , the real parts vanish and the critical momentum k_c further develops. We provide an example in figure 8, where the temperature T , magnetic field B , and permittivity ε_e are the same as those in figure 7. The only difference is we switch on axial relaxation with $M/b = 0.1$. One can find that axial relaxation forces the real part to disappear, and thus figure 8 becomes qualitatively similar to figure 6, instead of figure 7. In other words, axial charge relaxation favours the scenario with a k -gap rather than that with a frequency gap.

5.3 Properties of CMW and screened conductivity in holographic WSM

We finally study the properties of the CMW in a strongly-coupled WSM. When the magnetic field is not too strong and the electric charge and axial charge slowly dissipate, the dispersion

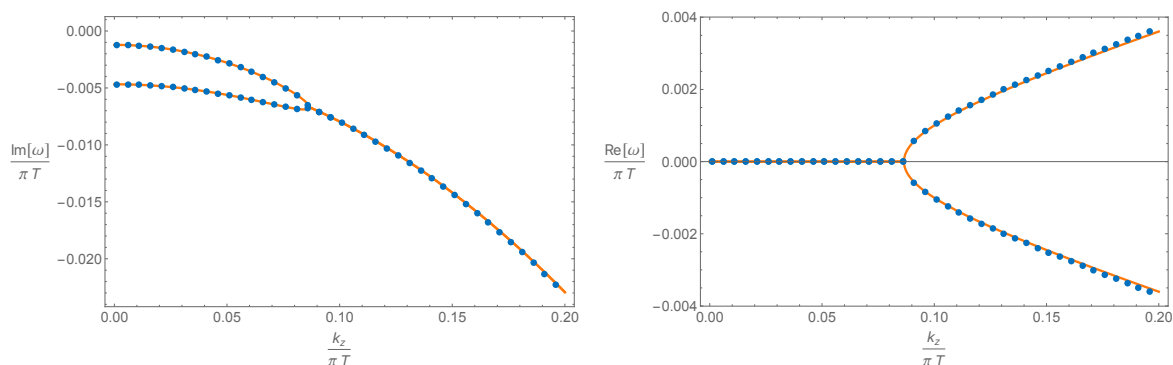


Figure 8. Lowest QNMs with $\tilde{B} = 0.005$, $\lambda_e/(\pi T) = 10^{-3}$, $\tilde{b} = 1$ and $M/b = 0.1$. The numerical results are represented by the numerical points while the prediction from quasi-hydrodynamics eq. (5.2) by solid lines.

relations of the CMW are precisely described by the quasi-hydrodynamic theory presented in section 2. Therefore, in such limit, we can directly use the quasi-hydrodynamic expressions eq. (5.2) to illustrate our results in figure 9.

As shown in eq. (5.2), in general the dispersion of the lowest modes ω_{\pm} has a real part which corresponds to the characteristic energy of the excitation and a imaginary part describing its attenuation rate or lifetime. Without loss of generality, we focus on ω_{-} and define

$$\omega_{-}(k_z) = -\Omega(k_z) - i\gamma(k_z), \quad (5.4)$$

where the minus sign in the real part indicates it propagates along the opposite direction with respect to the z axis. $\Omega(k_z)$ and $\gamma(k_z)$ depend on the parameters B, ε_e and Γ . Importantly, we define the ratio Ω/γ as a good indicator to establish the nature of the excitations. For $\Omega/\gamma \gg 1$, the modes are underdamped and eventually propagating. On the contrary, for $\Omega/\gamma \ll 1$, the modes are overdamped and they are not able to propagate. This condition will obviously render their experimental detection very hard.

The magnetic field B plays the most crucial role in controlling the ratio Ω/γ . In the small B regime, there is a k -gap in the real part of the dispersion. As B increases, the k -gap disappears and the absolute value of the real part increases with B . Correspondingly, Ω/γ at $k_z = 0$ remains zero below a critical value of the magnetic field and can reach very high values when the magnetic field is strong, which indicates that the overdamped wave becomes underdamped. As a concrete example, we take $\varepsilon_e = 100$ and $\Gamma = 1/1000$ (in unit $\pi T = 1$) to show the effects of B in the first and second rows in figure 9.

Both the energy of the CMW and the ratio Ω/γ are not very sensitive to the permittivity ε_e . As shown in the third row in figure 9, when we fix $B = 0.1$ and $\Gamma = 1/1000$ (in unit $\pi T = 1$), the behavior of CMW remains qualitatively similar as ε_e ranges from 10^2 to 10^4 .

The relaxation of the axial charge tends to destroy the CMW at small wave-vector, and consequently leads to a k -gap in the spectrum. For example, in the last row in figure 9 we take $B = 0.1$ and $\varepsilon_e = 100$ (in unit $\pi T = 1$) to demonstrate the effects of axial relaxation. It appears clear that a k -gap develops and then increases with Γ , while Ω/γ decreases monotonically to zero, which gradually makes the CMW overdamped and hence difficult to detect with experimental probes.

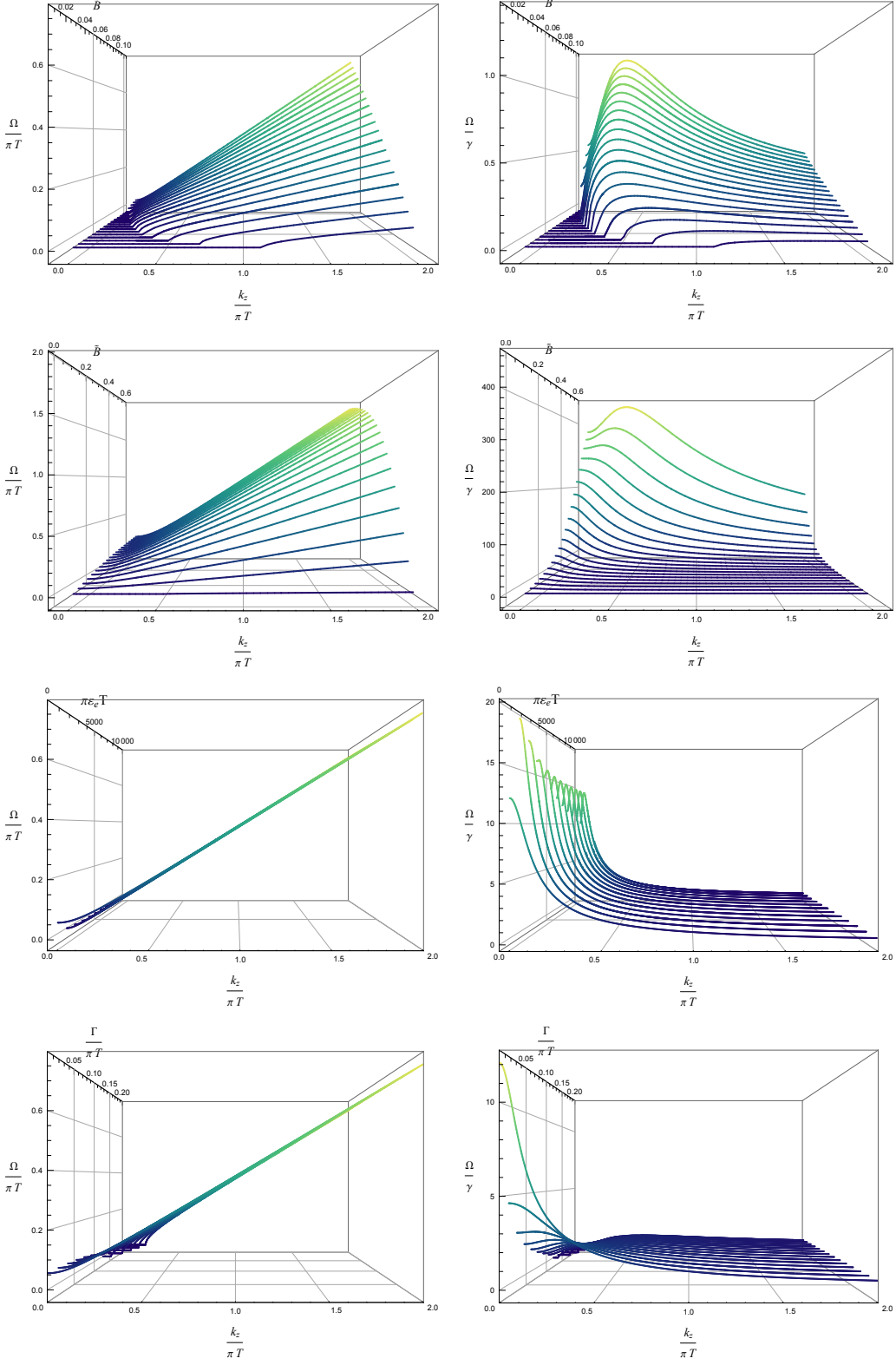


Figure 9. Waterfall plots for the real part of the dispersion relation $\text{Re}(\omega) \equiv -\Omega$ (Left) and the ratio $\Omega/\gamma \equiv \text{Re}(\omega)/\text{Im}(\omega)$ (Right) as a function of the wave-vector k_z and the magnetic field (rows 1–2), permittivity (row 3), and axial relaxation (row 4) respectively.

In addition to the damped CMW, another observable that is accessible from experiments is the screened AC conductivity defined by

$$\sigma_{\text{sc}}(\omega, \vec{k} = 0) = \frac{\sigma(\omega, \vec{k} = 0)}{\epsilon(\omega, \vec{k} = 0)} = \frac{\sigma(\omega, \vec{k} = 0)}{1 - \frac{\lambda_e}{i\omega} \sigma(\omega, \vec{k} = 0)}, \quad (5.5)$$

where $\sigma(\omega, \vec{k} = 0)$ is the bare AC conductivity computed from eq. (B.12) with infalling boundary conditions. Since the CMW is defined from the condition $\epsilon(\omega, \vec{k} = 0) = 0$, its signature should emerge in the conductivity when the imaginary part is small enough. As a result, $\sigma_{\text{sc}}(\omega, \vec{k} = 0)$ is a good observable to detect the magnitude of Ω/γ and to observe the CMW when it is underdamped.

As shown in figure 10, both the real and imaginary parts of $\sigma_{\text{sc}}(\omega)$ present qualitatively different behaviors depending on whether Ω/γ is large or small. In the real Weyl semimetals, the axial charge can be nearly conserved [24] and for simplicity, we take the $\Gamma = 0$ limit in order to focus on the screening effect. The magnetic field is fixed as $\tilde{B} = 0.05$, and we dial the strength of the Coulomb interactions, i.e., $\lambda_e = \epsilon_e^{-1}$. Increasing λ_e , the location of the pole on the complex plane, defined from the condition $\epsilon(\omega, \vec{k} = 0) = 0$, moves towards larger values as shown by the blue curve in the upper left plot of figure 10. On the contrary, the ratio Ω/γ decreases with it as shown in the corresponding upper right plot. Regarding the screened conductivity, when the magnitude of Ω/γ is sufficiently large, the real part of σ_{sc} presents a sharp resonance peak located at approximately, but not exactly, $\text{Re}[\omega(0)]$. When the magnitude of Ω/γ diminishes, the width of the resonance peak increases and the response becomes incoherent and flat. A similar behavior is found in the imaginary part. Intuitively, the features found in the conductivity are just related to the nature of the corresponding excitation which needs to be underdamped to produce a nice peak feature in the conductivity, and therefore be detectable.

We summarize this section with a contour plot of the ratio Ω/γ at $\Gamma = 0$ and $k_z = 0$, which is a reasonable approximation compared with the realistic Weyl semimetals. As shown in figure 11, when the magnetic field is small, i.e., $\tilde{B} \lesssim 0.02$, the CMW is always overdamped with $\Omega/\gamma \lesssim 10$ and decays exponentially to zero at long wavelengths, $k_z \rightarrow 0$. In the strong Coulomb interaction limit $\lambda_e \rightarrow \infty$ ($\epsilon_e \rightarrow 0$), the CMW is also overdamped due to charge decay. On the contrary, when the parameters are chosen to be above the contour line $\Omega/\gamma = 20$, the CMW is underdamped and still propagates at long wavelength, leading to an observable peak in the real part of the screened AC conductivity σ_{sc} .

6 Conclusions

Using hydrodynamics and bottom-up holography, we have performed a comprehensive study of the dispersion relation of collective chiral magnetic waves in strongly-coupled Weyl semimetals. In both frameworks, we have included the effects of axial charge relaxation and Coulomb interactions. Moreover, we have explicitly verified that the two methods give consistent results.

Using the holographic model as the underlying microscopic theory, we have first verified that the magnetic field does not affect the phase diagram in the probe limit. Then, we observed that the axial relaxation time τ_5 becomes longer in the Weyl semimetal phase than

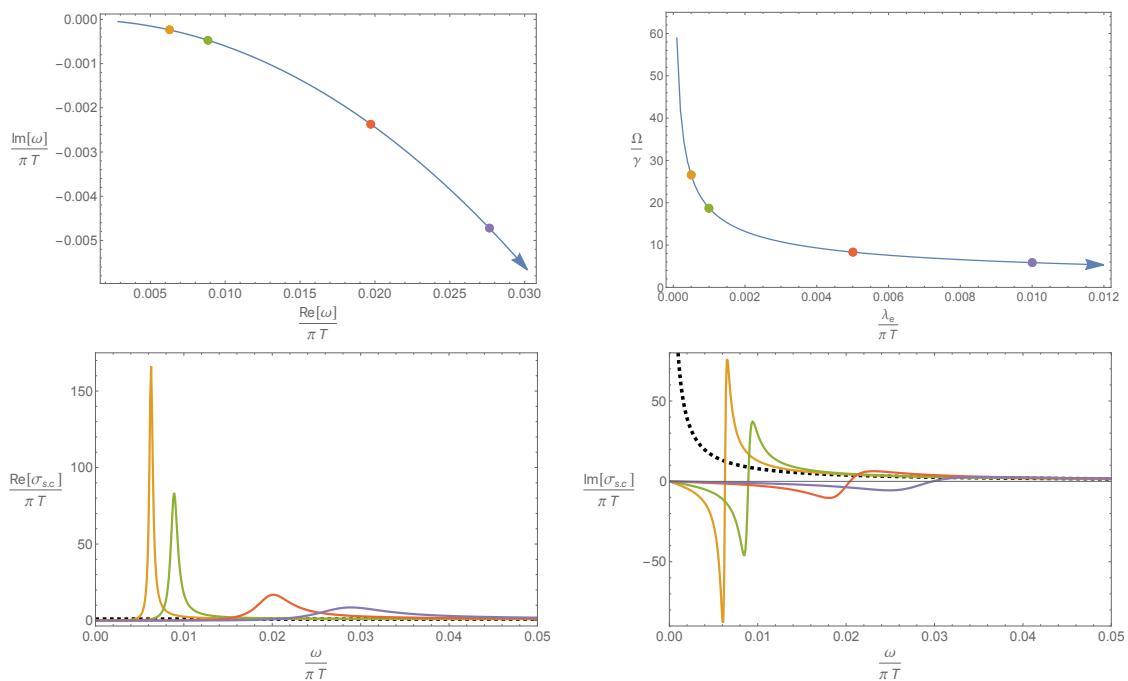


Figure 10. *Top:* location shift of the lowest pole on the complex plane and the ratio Ω/γ by dialing the EM strength λ_e in the direction of the arrow. *Bottom:* real and imaginary parts of the optical screened conductivity σ_{sc} for the corresponding parameters.

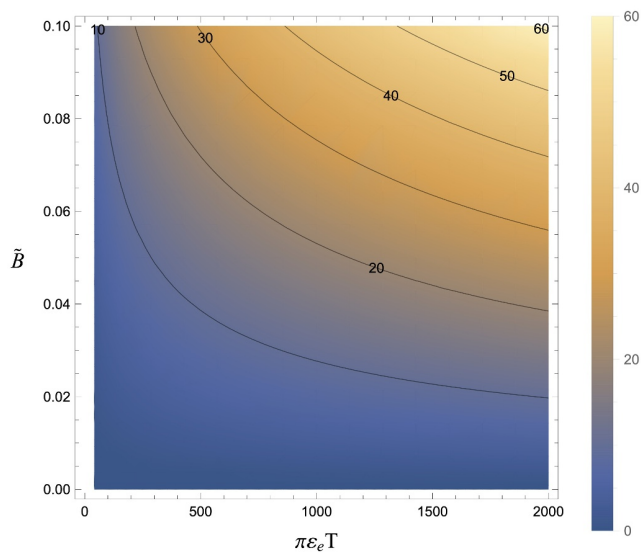


Figure 11. Contour plot of Ω/γ at $\Gamma = 0$ and $k_z = 0$, in the ϵ_e - \tilde{B} plane.

in the trivial semimetal one, which indicates that the Weyl nodes separation tends to restore axial charge conservation. Consequently, we argued that a longer τ_5 would facilitate the observation of chiral magnetic waves as underdamped collective excitations, making Weyl semimetals a possibly more promising experimental platform for their identification than heavy ion collisions. We also notice that in Weyl semimetal experiments, the behavior of negative longitudinal magnetoresistance [24, 50] indicates the presence of a large axial relaxation time.

Coulomb interactions, that are realized in holography using mixed boundary conditions for the bulk gauge field, modify the diffusion of vector charge fluctuations into a relaxation of the latter which is governed by the electric conductivity. However, Coulomb interactions also induce an energy gap (plasma frequency) that makes the dynamics of chiral magnetic waves more complicated. Now, different regimes can appear in which the dispersion relation of the chiral magnetic waves display a gap either in energy or in wave-vector, depending on which of the parameters dominate. We have confirmed that the hydrodynamic theory considered capture all these effects well and indeed is quantitatively consistent with the numerical data from holography.

Finally, in order to verify whether chiral magnetic waves could be observable as underdamped excitations, we have investigated the ratio between the energy and relaxation rate, i.e., Ω/γ , and focused on the effects of the magnetic field, Coulomb interactions, and axial relaxation that are the typical measurable parameters in Weyl semimetals. To provide a more direct test of the aforementioned ratio, we also computed the screened conductivity in the holographic Weyl semimetal model and showed a one-to-one correspondence with the damped propagating chiral magnetic wave. As expected, when the chiral magnetic wave is underdamped, we observe a peak in the screened conductivity σ_{sc} that could be in principle directly accessible to experiments.

Many questions are left to be explored. It would be interesting to study the possibility of observing CMW in holographic nodal line semimetals [68–70], as well as to explore the observable effects of CMW in neutron stars [71, 72], or even in our early universe [73, 74].

Moreover, it would be fruitful to investigate in more detail the dielectric response and the properties of the plasmon frequency with respect to magnetic field in topological semimetals [75], which might be another feasible method to detect CMW. Additionally, it is known that there might exist other types of waves in Weyl semimetals due to the torsional strain deformations, e.g., chiral sound wave [76], chiral density wave [77]. It would be interesting to study these waves in the holographic Weyl semimetal model by introducing the effects of elasticity and strain (see [78]).

Acknowledgments

We thank Karl Landsteiner and Igor Shovkovy for useful comments on a preliminary draft of this work. Y.A., M.B. and X.-M.W. acknowledge the support of the Shanghai Municipal Science and Technology Major Project (Grant No.2019SHZDZX01). M.B. acknowledges the sponsorship from the Yangyang Development Fund. Y.L. is supported by the National Natural Science Foundation of China grant No.11875083, 12375041. X.-M.W. is supported by the China Postdoctoral Science Foundation (Grant No. 2023M742296).

A Equations of motion

The action for the holographic WSM model is given by

$$\begin{aligned}
 S = \int d^5x \sqrt{-g} & \left[\frac{1}{2\kappa^2} \left(R + \frac{12}{L^2} \right) \right. \\
 & \left. - \frac{1}{4e^2} \mathcal{F}^2 - \frac{1}{4e^2} F^2 - (D_\mu \Phi)^* (D^\mu \Phi) - V(\Phi) + \epsilon^{\mu\nu\rho\sigma\tau} A_\mu \left(\frac{\alpha}{3} (F_{\nu\rho} F_{\sigma\tau} + 3\mathcal{F}_{\nu\rho} \mathcal{F}_{\sigma\tau}) \right) \right],
 \end{aligned} \tag{A.1}$$

where $V(\Phi) = m^2 |\Phi|^2$ is the potential of the scalar. We consider the probe limit, i.e., the gravitational background is fixed to be the thermal AdS-Schwarzschild background. The equations of motion for the matter fields are

$$\begin{aligned}
 \nabla_\nu \mathcal{F}^{\nu\mu} + 2\alpha \epsilon^{\mu\tau\beta\rho\sigma} F_{\tau\beta} \mathcal{F}_{\rho\sigma} &= 0, \\
 \nabla_\nu F^{\nu\mu} + \epsilon^{\mu\tau\beta\rho\sigma} \left[\alpha (F_{\tau\beta} F_{\rho\sigma} + \mathcal{F}_{\tau\beta} \mathcal{F}_{\rho\sigma}) \right] + iq [\Phi (D^\mu \Phi)^* - \Phi^* (D^\mu \Phi)] &= 0, \\
 D_\mu D^\mu \Phi - m^2 \Phi &= 0.
 \end{aligned}$$

In the manuscript, we have taken $2\kappa^2 = 1$ and $e^2 = 1$.

A.1 Equations for the longitudinal fluctuations

We consider the longitudinal sector and switch on the following fluctuations

$$\delta a_t, \quad \delta a_z, \quad \delta v_t, \quad \delta v_z, \quad \delta \phi_1, \quad \delta \phi_2, \tag{A.2}$$

where $\delta \phi_1$ and $\delta \phi_2$ are the real and imaginary parts of the complex scalar fluctuation $\delta \Phi$, with the definition $\delta \Phi \equiv \delta \phi_1 + i \delta \phi_2$. We work in Fourier space by decomposing the fluctuations as

$$\begin{aligned}
 \delta a_t &= a_t(r) e^{-i\omega t + ik_z z}, & \delta a_z &= a_z(r) e^{-i\omega t + ik_z z}, \\
 \delta v_t &= v_t(r) e^{-i\omega t + ik_z z}, & \delta v_z &= v_z(r) e^{-i\omega t + ik_z z}, \\
 \delta \phi_1 &= \phi_1(r) e^{-i\omega t + ik_z z}, & \delta \phi_2 &= \phi_2(r) e^{-i\omega t + ik_z z}.
 \end{aligned} \tag{A.3}$$

In the probe limit, the second-order equations of motions for the fluctuations are

$$\begin{aligned}
 a_t'' + \frac{3a_t'}{r} - \left(\frac{k_z^2}{r^2 u} + \frac{2q^2 \phi^2}{u} \right) a_t + \frac{8\alpha B v_z'}{r^3} - \frac{\omega k_z}{r^2 u} a_z - \frac{2iq\omega\phi}{u} \phi_2 &= 0, \\
 a_z'' + \left(\frac{1}{r} + \frac{u'}{u} \right) a_z' + \left(\frac{\omega^2}{u^2} - \frac{2q^2 \phi^2}{u} \right) a_z + \frac{8\alpha B}{ru} v_t' + \frac{\omega k_z}{u^2} a_t - \frac{4q^2 A_z \phi}{u} \phi_1 + \frac{2iqk_z \phi}{u} \phi_2 &= 0, \\
 v_t'' + \frac{3}{r} v_t' - \frac{k_z^2}{r^2 u} v_t + \frac{8\alpha B}{r^3} a_z' - \frac{\omega k_z}{r^2 u} v_z &= 0, \\
 v_z'' + \left(\frac{1}{r} + \frac{u'}{u} \right) v_z' + \frac{\omega^2}{u^2} v_z + \frac{8\alpha B}{ru} a_t' + \frac{\omega k_z}{u^2} v_t &= 0, \\
 \phi_1'' + \left(\frac{3}{r} + \frac{u'}{u} \right) \phi_1' + \left(\frac{\omega^2}{u^2} - \frac{m^2}{u} - \frac{k_z^2}{r^2 u} - \frac{q^2 A_z^2}{r^2 u} \right) \phi_1 - \frac{2qA_z}{r^2 u} (q\phi a_z - ik_z \phi_2) &= 0, \\
 \phi_2'' + \left(\frac{3}{r} + \frac{u'}{u} \right) \phi_2' + \left(\frac{\omega^2}{u^2} - \frac{m^2}{u} - \frac{k_z^2}{r^2 u} - \frac{q^2 A_z^2}{r^2 u} \right) \phi_2 - iq\phi \left(\frac{\omega a_t}{u^2} + \frac{k_z a_z}{r^2 u} \right) - \frac{2iqk_z A_z}{r^2 u} \phi_1 &= 0.
 \end{aligned} \tag{A.4}$$

There are also two first-order equations (constraints)

$$\begin{aligned} \frac{\omega}{u}v'_t + \frac{k_z}{r^2}v'_z + \frac{8\alpha B}{r^3u}(k_za_t + \omega a_z) &= 0, \\ \frac{\omega}{u}a'_t + \frac{k_z}{r^2}a'_z + \frac{8\alpha B}{r^3u}(k_zv_t + \omega v_z) + 2iq(\phi\phi'_2 - \phi'\phi_2) &= 0. \end{aligned} \quad (\text{A.5})$$

A.2 Equations for the transverse fluctuations

In order to compute the anomalous Hall conductivity σ_{AHE} , we consider the transverse sector and switch on the fluctuations at $k_z = 0$ as follows

$$\delta a_x, \quad \delta a_y, \quad \delta v_x, \quad \delta v_y. \quad (\text{A.6})$$

We consider only homogeneous perturbations, hence

$$\begin{aligned} \delta a_x &= a_x(r)e^{-i\omega t}, & \delta a_y &= a_y(r)e^{-i\omega t}, \\ \delta v_x &= v_x(r)e^{-i\omega t}, & \delta v_y &= v_y(r)e^{-i\omega t}. \end{aligned} \quad (\text{A.7})$$

The equations for these perturbations read

$$\begin{aligned} v''_x + \left(\frac{1}{r} + \frac{u'}{u}\right)v'_x + \frac{\omega^2}{u^2}v_x + \frac{8i\alpha\omega}{ru}A'_zv_y &= 0, \\ v''_y + \left(\frac{1}{r} + \frac{u'}{u}\right)v'_y + \frac{\omega^2}{u^2}v_y - \frac{8i\alpha\omega}{ru}A'_zv_x &= 0, \\ a''_x + \left(\frac{1}{r} + \frac{u'}{u}\right)a'_x + \left(\frac{\omega^2}{u^2} - \frac{2q^2\phi^2}{u}\right)a_x + \frac{8i\alpha\omega}{ru}A'_za_y &= 0, \\ a''_y + \left(\frac{1}{r} + \frac{u'}{u}\right)a'_y + \left(\frac{\omega^2}{u^2} - \frac{2q^2\phi^2}{u}\right)a_y - \frac{8i\alpha\omega}{ru}A'_za_x &= 0. \end{aligned} \quad (\text{A.8})$$

By changing variables to $v_{\pm} \equiv v_x \pm i v_y$, the equations simplify into

$$v''_{\pm} + \left(\frac{1}{r} + \frac{u'}{u}\right)v'_{\pm} + \frac{\omega^2}{u^2}v_{\pm} \pm \frac{8\alpha\omega}{ru}A'_zv_{\pm} = 0. \quad (\text{A.9})$$

In order to compute the DC σ_{AHE} , we expand v_{\pm} around $\omega = 0$ as

$$v_{\pm} = \left(1 - \frac{r_h^4}{r^4}\right)^{-\frac{i\omega}{4r_h}} \left(v_{\pm}^{(0)} + \omega v_{\pm}^{(1)} + \dots\right). \quad (\text{A.10})$$

After imposing the regularity condition near the horizon, we obtain the solutions $v_{\pm}^{(0)} = c_0$ and

$$v_{\pm}^{(1)} = -\int_r^{\infty} dx \frac{c_0}{x^3 f} \left[\frac{ix^3 f'}{4r_h} - ir_h \mp 8\alpha(A_z - A_z(r_h)) \right]. \quad (\text{A.11})$$

Therefore, we obtain the Green's function $G_{\pm} = \omega(\pm 8\alpha(b - A_z(r_h)) + ir_h)$ and

$$\sigma_{xy} = \frac{G_+ - G_-}{2\omega} = 8\alpha(b - A_z(r_h)), \quad (\text{A.12})$$

which is the Hall conductivity for the covariant current. In order to consider the consistent current, we have to add the contribution from the Chern-Simons term and finally

$$\sigma_{\text{AHE}} = 8\alpha b - \sigma_{xy} = 8\alpha A_z(r_h). \quad (\text{A.13})$$

In the presence of magnetic field B , σ_{AHE} is a function of B through the horizon value of A_z .

A.3 On-shell action

The on-shell action for the fluctuations is necessary to define the proper susceptibilities and conductivities. The renormalized action of the boundary field theory is given by

$$S_{\text{ren}} = S + S_{\text{bnd}} \quad (\text{A.14})$$

with S defined in eq. (3.1) and

$$S_{\text{bnd}} = \frac{1}{\kappa^2} \int_{r=r_\infty} d^4x \sqrt{-\gamma} K - \frac{1}{2\kappa^2} \int_{r=r_\infty} d^4x \sqrt{-\gamma} \left[6 + \frac{1}{2}R + \dots \right] \\ + \frac{\log r}{4} \int_{r=r_\infty} d^4x \sqrt{-\gamma} \left[\mathcal{F}_{\mu\nu} \mathcal{F}^{\mu\nu} + F_{\mu\nu} F^{\mu\nu} + |D_m \Phi|^2 + \frac{1}{3} |\Phi|^4 \right] \quad (\text{A.15})$$

where γ_{ab} is the induced metric on the boundary. K and R are the extrinsic and intrinsic curvatures respectively.

Substituting the fluctuations at $\omega \neq 0, k_z = 0$ into the total renormalized action (A.14), we obtain the relevant part in the renormalized on-shell action

$$S_{\text{o.s.}} \supset \int \frac{d\omega}{2\pi} dx^3 \left[-2a_t^{(0)}(-\omega) a_t^{(2)}(\omega) + 2a_z^{(0)}(-\omega) a_z^{(2)}(\omega) \right. \\ \left. - 2v_t^{(0)}(-\omega) v_t^{(2)}(\omega) + 2v_z^{(0)}(-\omega) v_z^{(2)}(\omega) \right. \\ \left. + \mathcal{O}(\omega^2) + \text{contact terms} \right]. \quad (\text{A.16})$$

Note that there is a factor 2 which is crucial to properly define the susceptibilities and DC conductivities.

B Susceptibilities and conductivities

The total axial charge susceptibility χ_A^{tot} is defined from the correlation function of the axial charge density, i.e., $\chi_A^{\text{tot}} = \langle \rho_A \rho_A \rangle_R |_{\omega=k=0}$. It can be obtained in holography by solving

$$a_t'' + \frac{3}{r} a_t' - \left(\frac{64B^2 \alpha^2}{r^4 u} + \frac{2q^2 \phi^2}{u} \right) a_t = 0. \quad (\text{B.1})$$

The asymptotic expansion of a_t near the boundary is given by

$$a_t(r) = a_t^{(0)} - \frac{q^2 M^2 a_t^{(0)}}{r^2} \ln r - \frac{a_t^{(2)}}{r^2} + \dots, \quad (\text{B.2})$$

hence $\chi_A^{\text{tot}} = \frac{2a_t^{(2)}}{a_t^{(0)}}$. χ_A in the constitutive equations is obtained by taking $\phi = 0$ during the computation.

The total vector charge susceptibility χ_V^{tot} is defined from the correlation function of the charge density, i.e., $\chi_V^{\text{tot}} = \langle \rho_V \rho_V \rangle_R |_{\omega=k=0}$, which can be extracted from

$$v_t'' + \frac{3}{r} v_t' + \frac{8B\alpha}{r^3} a_z' = 0, \\ a_z'' + \left(\frac{1}{r} + \frac{u'}{u} \right) a_z' + \frac{8B\alpha}{ru} v_t' - \frac{2q^2 \phi^2}{u} a_z = 0. \quad (\text{B.3})$$

The UV expansions of the relevant bulk fields are given by

$$\begin{aligned} a_z(r) &= a_z^{(0)} - \frac{q^2 M^2 a_z^{(0)}}{r^2} \ln r + \frac{a_z^{(2)}}{r^2} + \dots, \\ v_t(r) &= v_t^{(0)} - \frac{v_t^{(2)}}{r^2} + \dots. \end{aligned} \tag{B.4}$$

This implies that $\chi_V^{\text{tot}} = \frac{2v_t^{(2)}}{v_t^{(0)}}$ with the sourceless boundary condition $a_z^{(0)} = 0$. χ_V in the constitutive equations is obtained by taking $\phi = 0$ during the computation.

The total longitudinal DC axial conductivity σ_{DC}^A is defined from the correlation function of the longitudinal axial current, i.e., $\sigma_{\text{DC}}^A = \text{Im} \frac{1}{\omega} \langle J_A^z J_A^z \rangle_R |_{k_z=0, \omega \rightarrow 0}$, which can be obtained from

$$a_z'' + \left(\frac{1}{r} + \frac{u'}{u} \right) + \left(\frac{\omega^2}{u^2} - \frac{2q^2 \phi^2}{u} - \frac{64B^2 \alpha^2}{r^4 u} \right) a_z = 0. \tag{B.5}$$

The UV expansion for a_z reads

$$a_z(r) = a_z^{(0)} - \frac{q^2 M^2 a_z^{(0)}}{r^2} \ln r + \frac{a_z^{(2)}}{r^2} + \dots, \tag{B.6}$$

and gives $\sigma_{\text{DC}}^A = 2 \lim_{\omega \rightarrow 0} \text{Im} \left[\frac{a_z^{(2)}}{a_z^{(0)}} \right]$. σ_A in the constitutive equations is obtained by taking $\phi = 0$ during the computation.

The total longitudinal DC electric conductivity σ_{DC}^V can be computed analytically due to the existence of the radial conserved quantity when $\omega = 0$. It can be solved from the coupled equations

$$\begin{aligned} v_z'' + \left(\frac{1}{r} + \frac{u'}{u} \right) + \frac{8B\alpha}{ru} a_t' &= 0, \\ a_t'' + \frac{3}{r} a_t' + \frac{8B\alpha}{r^3} v_z' - \frac{2q^2 \phi^2}{u} a_t &= 0. \end{aligned} \tag{B.7}$$

From the first equation in eq. (B.7) we have the radial conserved quantity $J = -ruv_z' - 8B\alpha a_t$ satisfying $\partial_r J = 0$, which means $J|_{r \rightarrow \infty} = J|_{r \rightarrow r_0} \equiv j$ and σ_{DC}^V can be computed at the horizon. Near the horizon,

$$\begin{aligned} v_z &= -\frac{E}{4\pi T} \ln(r - r_0) + \dots, \\ a_t &= -\frac{2E(8B\alpha)}{(4\pi T)r_0^2 (q\phi_h)^2} + \dots, \end{aligned} \tag{B.8}$$

and therefore

$$\sigma_{\text{DC}}^V = \frac{j}{E} = \pi T + \frac{32B^2 \alpha^2}{\pi^3 T^3 q^2 \phi_h^2}. \tag{B.9}$$

Alternatively, one can obtain the same result from numerics, by switching on a sub-leading term $a_1(r - r_0)$ in a_t in eq. (B.8), where a_1 is determined from the UV expansion

$$\begin{aligned} a_t(r) &= a_t^{(0)} - \frac{q^2 M^2 a_t^{(0)}}{r^2} \ln r - \frac{a_t^{(2)}}{r^2} + \dots, \\ v_z(r) &= v_z^{(0)} + \frac{v_z^{(2)}}{r^2} \dots, \end{aligned} \tag{B.10}$$

with the sourceless boundary condition $a_i^{(0)} = 0$. As a result, $\sigma_{\text{DC}}^V = \frac{2v_z^{(2)}}{E}$ is consistent with the analytic result eq. (B.9).

The axial charge relaxation effects on transport are negligible when $\tau T \rightarrow \infty$. In this limit, the equations can be solved analytically as a function of B/T^2 , leading to the quantum critical conductivities in the presence of B , i.e.

$$\sigma_A = \sigma_V = \sigma = \frac{\pi^2 T}{8} \beta^2 \sec\left(\frac{\pi}{2} \sqrt{1-\beta^2}\right) \frac{\Gamma\left[\frac{3-\sqrt{1-\beta^2}}{4}\right] \Gamma\left[\frac{3+\sqrt{1-\beta^2}}{4}\right]}{\Gamma\left[\frac{5-\sqrt{1-\beta^2}}{4}\right] \Gamma\left[\frac{5+\sqrt{1-\beta^2}}{4}\right]} \quad (\text{B.11})$$

with $\beta = \frac{8B\alpha}{\pi^2 T^2}$. When $\beta \ll 1$, we have $\sigma = \pi T(1 - \frac{\log 2}{2} \beta^2 + \mathcal{O}(\beta^4))$.

Finally, to compute the AC conductivity $\sigma_V(\omega)$ at zero momentum $\vec{k} = 0$ without axial relaxation, i.e., $\phi = 0$, we solve the ODE

$$v_z'' + \left(\frac{1}{r} + \frac{u'}{u}\right) v_z' + \left(\frac{\omega^2}{u^2} - \frac{64\alpha^2 B^2}{r^4 u}\right) v_z = 0 \quad (\text{B.12})$$

with the infalling boundary condition of v_z at the horizon.

C Coulomb screening, density-density correlation function and conductivities

In the following, we give a brief introduction to Coulomb screening effects on electric susceptibility (density-density correlation function) and electric conductivity (current-current correlation function). We follow the textbook [37] and use SI units.

For simplicity, we start from electrostatics in the jellium model. Switching on an external potential $v_{\text{ext}}(\vec{x})$, we can write down the energy functional $E[\rho]$ of the charge density $\rho(\vec{x})$ of the electrons with number density $n(\vec{x})$, and each electron carries charge $-e$ that defines the electric charge density $\rho(\vec{x}) = -en(\vec{x})$,

$$\begin{aligned} E[\rho] &= E_{\text{int}}[\rho] + \int d\vec{x} \rho(\vec{x}) v_{\text{ext}}(\vec{x}), \\ E_{\text{int}}[\rho] &= E_{\text{int}}[\rho_0] + \frac{1}{2} \int d\vec{x} \int d\vec{x}' \delta\rho(\vec{x}) \frac{\delta^2 E_{\text{int}}[\rho]}{\delta\rho(\vec{x}) \delta\rho(\vec{x}')} \Big|_{\rho_0} \delta\rho(\vec{x}') + \dots \end{aligned} \quad (\text{C.1})$$

where in the Taylor expansion the linear term vanishes at equilibrium, $\rho(\vec{x}) = \rho_0$.

Minimizing the energy functional with respect to $\rho(\vec{x})$, we obtain

$$\frac{\delta E[\rho]}{\delta\rho(\vec{x})} = \int d\vec{x}' \frac{\delta^2 E_{\text{int}}[\rho]}{\delta\rho(\vec{x}) \delta\rho(\vec{x}')} \Big|_{\rho_0} \delta\rho(\vec{x}') + v_{\text{ext}}(\vec{x}) = 0 \quad (\text{C.2})$$

that defines the response function to the external source v_{ext}

$$\delta\rho(\vec{x}) = \int d\vec{x}' \chi(\vec{x}, \vec{x}') v_{\text{ext}}(\vec{x}'), \quad (\text{C.3})$$

and further the electric charge density-density correlation function as

$$\chi(\vec{x}, \vec{x}') = - \left[\frac{\delta^2 E_{\text{int}}[\rho]}{\delta\rho(\vec{x}) \delta\rho(\vec{x}')} \Big|_{\rho_0} \right]^{-1}. \quad (\text{C.4})$$

Then, we perform the Fourier transformation and define the density-density correlation function in the momentum space

$$\chi(\vec{k}) \equiv \int d\vec{x} \chi(\vec{x}) e^{-i\vec{k}\cdot\vec{x}}, \quad \text{with} \quad \delta\rho(\vec{k}) = \chi(\vec{k}) v_{\text{ext}}(\vec{k}). \quad (\text{C.5})$$

In order to distinguish the quantities with or without Coulomb screening, we use a normal symbol for the unscreened observables (non-interacting/bare quantities), while using a subscript “sc” for the screened ones (interacting/renormalized quantities).

We consider the energy functional

$$E_{\text{int}}[\rho] = \frac{1}{2} \int d\vec{x} \int d\vec{x}' \rho(\vec{x}) \frac{\lambda_e}{4\pi|\vec{x} - \vec{x}'|} \rho(\vec{x}') + T_S[\rho], \quad (\text{C.6})$$

where the first term represents the energy due to the Coulomb potential with the strength tunable that is proportional to λ_e and $T_S[\rho]$ the energy for non-interacting electrons. For the non-interacting electrons, the density-density correlation only comes from $T_S[\rho]$ that is defined as

$$\chi(\vec{x}, \vec{x}') = - \left[\frac{\delta^2 T_S[\rho]}{\delta\rho(\vec{x}) \delta\rho(\vec{x}')} \Big|_{\rho_0} \right]^{-1}. \quad (\text{C.7})$$

Making a comparison between the density-density correlation function with and without Coulomb interactions in momentum space, we find

$$-\chi_{\text{sc}}^{-1}(\vec{k}) = \frac{\lambda_e}{|\vec{k}|^2} - \chi^{-1}(\vec{k}). \quad (\text{C.8})$$

After taking into account the frequency dependence to consider dynamical processes, we finally obtain the dynamical density-density correlation function in the random-phase approximation (RPA) that we ignore the exchange-correlation contribution in the energy functional and consider the effect of Coulomb interaction at Hartree level,

$$\chi_{\text{sc}}(\omega, \vec{k}) = \chi_{\text{RPA}}(\omega, \vec{k}) = \frac{\chi(\omega, \vec{k})}{1 - (\lambda_e/|\vec{k}|^2)\chi(\omega, \vec{k})}. \quad (\text{C.9})$$

On the left side, $\chi_{\text{sc}}(\omega, \vec{k})$ is the screened density-density correlation function in response to the external potential v_{ext} with Coulomb potential. On the right side, $\chi(\omega, \vec{k})$ is the unscreened density-density correlation in response to the external potential v_{ext} without Coulomb potential.

We then discuss the different meanings of the poles of $\chi(\omega, \vec{k})$ and $\chi_{\text{sc}}(\omega, \vec{k})$ in holography, based on eq. (C.9). To compute the poles of $\chi(\omega, \vec{k})$, we take the vanishing Dirichlet boundary condition for the field at the boundary. This means that we switch off the external source for the operator $\delta\rho$, e.g. $v_{\text{ext}} = 0$. On the contrary, to compute the poles of $\chi_{\text{sc}}(\omega, \vec{k})$, we take the dynamical dielectric function to vanish

$$\epsilon(\omega, \vec{k}) \equiv 1 - (\lambda_e/|\vec{k}|^2)\chi(\omega, \vec{k}) = 0, \quad (\text{C.10})$$

which corresponds to the displacement field vanishing or the external charge ρ_{ext} vanishing, i.e. $\vec{D} = \rho_{\text{ext}} = 0$. In the zero wave-vector limit $\vec{k} \rightarrow 0$, $\epsilon(\omega = \Omega_{\text{pl}}, \vec{k} \rightarrow 0) = 0$ gives the

plasma frequency $\omega = \Omega_{\text{pl}}$. In the finite wave-vector \vec{k} regime, the dispersion relation of the plasma oscillations can be obtained from $\epsilon(\omega, \vec{k}) = 0$.

Let us move to discuss the screening effects on the longitudinal conductivity. To start with, we recall the Maxwell's equations

$$\vec{\nabla} \cdot \vec{D} = \rho_{\text{ext}}, \quad \vec{\nabla} \cdot \vec{E} = (\rho_{\text{int}} + \rho_{\text{ext}}) \equiv \rho_{\text{tot}} \quad (\text{C.11})$$

where the electric displacement field \vec{D} is related to the electric field \vec{E} via the dielectric function as

$$\vec{D} = \epsilon \vec{E}. \quad (\text{C.12})$$

Here we should be careful to define the conductivity since we can express $\vec{J} \equiv \vec{J}_{\text{int}}$ with respect to \vec{D} as well as \vec{E} as

$$\vec{J} = \sigma_{\text{sc}} \vec{D}, \quad \vec{J} = \sigma \vec{E}. \quad (\text{C.13})$$

In the first equation, the conductivity is defined with respect to the external field \vec{D} , then the Coulomb screening effect is included in the conductivity; while in the second equation, the current responds to the total electric field and the Coulomb screening effect is included in the electric field or the electric potential. Therefore, we can conclude that

$$\epsilon = \frac{\chi}{\chi_{\text{sc}}} = \frac{\sigma}{\sigma_{\text{sc}}} = \frac{\vec{D}}{\vec{E}} = \frac{V_{\text{ext}}}{V}, \quad (\text{C.14})$$

where the electric potential V_{ext}, V are defined from $\vec{D} = -\nabla V_{\text{ext}}$ and $\vec{E} = -\nabla V$ respectively.

Next, we can relate the conductivity σ with the dielectric function, via the continuity equation

$$\frac{\partial \rho}{\partial t} + \vec{\nabla} \cdot \vec{J} = 0, \quad (\text{C.15})$$

where both $\rho = -en \equiv \rho_{\text{int}}$ and $\vec{J} \equiv \vec{J}_{\text{int}}$ are the responses inside the matter. After Fourier transformation,

$$\rho(\omega, \vec{k}) = \frac{1}{\omega} \vec{k} \cdot \vec{J}(\omega, \vec{k}) = \frac{1}{\omega} \sigma(\omega, \vec{k}) (\vec{k} \cdot \vec{E}(\omega, \vec{k})). \quad (\text{C.16})$$

Recall that

$$\vec{D}(\omega, \vec{k}) = \epsilon(\omega, \vec{k}) \vec{E}(\omega, \vec{k}) = \vec{E}(\omega, \vec{k}) + \vec{P}(\omega, \vec{k}) \quad (\text{C.17})$$

where \vec{P} is the polarization field satisfying $\vec{\nabla} \cdot \vec{P} = -\rho_{\text{int}}/\epsilon_e$ with $\epsilon_e = 1/\lambda_e$. Combining eq. (C.16) and eq. (C.17), we finally obtain the relation

$$\epsilon(\omega, \vec{k}) = 1 - \frac{\lambda_e}{i\omega} \sigma(\omega, \vec{k}) \quad (\text{C.18})$$

and therefore the relation between the screened longitudinal conductivity σ_{sc} and the un-screened one σ as

$$\sigma_{\text{sc}}(\omega, \vec{k}) = \frac{\sigma(\omega, \vec{k})}{1 - \frac{\lambda_e}{i\omega} \sigma(\omega, \vec{k})}, \quad (\text{C.19})$$

which is also based on RPA.

Open Access. This article is distributed under the terms of the Creative Commons Attribution License ([CC-BY4.0](https://creativecommons.org/licenses/by/4.0/)), which permits any use, distribution and reproduction in any medium, provided the original author(s) and source are credited.

References

- [1] D.E. Kharzeev, J. Liao, S.A. Voloshin and G. Wang, *Chiral magnetic and vortical effects in high-energy nuclear collisions — A status report*, *Prog. Part. Nucl. Phys.* **88** (2016) 1 [[arXiv:1511.04050](https://arxiv.org/abs/1511.04050)] [[INSPIRE](#)].
- [2] K. Landsteiner, *Notes on Anomaly Induced Transport*, *Acta Phys. Polon. B* **47** (2016) 2617 [[arXiv:1610.04413](https://arxiv.org/abs/1610.04413)] [[INSPIRE](#)].
- [3] K. Fukushima, D.E. Kharzeev and H.J. Warringa, *The Chiral Magnetic Effect*, *Phys. Rev. D* **78** (2008) 074033 [[arXiv:0808.3382](https://arxiv.org/abs/0808.3382)] [[INSPIRE](#)].
- [4] M.A. Metlitski and A.R. Zhitnitsky, *Anomalous axion interactions and topological currents in dense matter*, *Phys. Rev. D* **72** (2005) 045011 [[hep-ph/0505072](https://arxiv.org/abs/hep-ph/0505072)] [[INSPIRE](#)].
- [5] J. Erdmenger, M. Haack, M. Kaminski and A. Yarom, *Fluid dynamics of R-charged black holes*, *JHEP* **01** (2009) 055 [[arXiv:0809.2488](https://arxiv.org/abs/0809.2488)] [[INSPIRE](#)].
- [6] N. Banerjee et al., *Hydrodynamics from charged black branes*, *JHEP* **01** (2011) 094 [[arXiv:0809.2596](https://arxiv.org/abs/0809.2596)] [[INSPIRE](#)].
- [7] G.M. Newman, *Anomalous hydrodynamics*, *JHEP* **01** (2006) 158 [[hep-ph/0511236](https://arxiv.org/abs/hep-ph/0511236)] [[INSPIRE](#)].
- [8] D.E. Kharzeev and H.-U. Yee, *Chiral Magnetic Wave*, *Phys. Rev. D* **83** (2011) 085007 [[arXiv:1012.6026](https://arxiv.org/abs/1012.6026)] [[INSPIRE](#)].
- [9] STAR collaboration, *Charge asymmetry dependency of π^+/π^- elliptic flow in Au + Au collisions at $\sqrt{s_{NN}} = 200$ GeV*, *J. Phys. Conf. Ser.* **389** (2012) 012035 [[arXiv:1211.3216](https://arxiv.org/abs/1211.3216)] [[INSPIRE](#)].
- [10] ALICE collaboration, *Charge-dependent anisotropic flow studies and the search for the Chiral Magnetic Wave in ALICE*, *Nucl. Phys. A* **931** (2014) 981 [[arXiv:1408.1043](https://arxiv.org/abs/1408.1043)] [[INSPIRE](#)].
- [11] STAR collaboration, *Observation of charge asymmetry dependence of pion elliptic flow and the possible chiral magnetic wave in heavy-ion collisions*, *Phys. Rev. Lett.* **114** (2015) 252302 [[arXiv:1504.02175](https://arxiv.org/abs/1504.02175)] [[INSPIRE](#)].
- [12] Y. Burnier, D.E. Kharzeev, J. Liao and H.-U. Yee, *Chiral magnetic wave at finite baryon density and the electric quadrupole moment of quark-gluon plasma in heavy ion collisions*, *Phys. Rev. Lett.* **107** (2011) 052303 [[arXiv:1103.1307](https://arxiv.org/abs/1103.1307)] [[INSPIRE](#)].
- [13] CMS collaboration, *Probing the chiral magnetic wave in pPb and PbPb collisions at $\sqrt{s_{NN}} = 5.02$ TeV using charge-dependent azimuthal anisotropies*, *Phys. Rev. C* **100** (2019) 064908 [[arXiv:1708.08901](https://arxiv.org/abs/1708.08901)] [[INSPIRE](#)].
- [14] ALICE collaboration, *Probing Chiral Magnetic Wave phenomena in Pb-Pb collisions with ALICE at the LHC*, *J. Phys. Conf. Ser.* **2586** (2023) 012025 [[INSPIRE](#)].
- [15] A. Jimenez-Alba, K. Landsteiner and L. Melgar, *Anomalous magnetoresponse and the Stückelberg axion in holography*, *Phys. Rev. D* **90** (2014) 126004 [[arXiv:1407.8162](https://arxiv.org/abs/1407.8162)] [[INSPIRE](#)].
- [16] K. Hattori, Y. Hirono, H.-U. Yee and Y. Yin, *MagnetoHydrodynamics with chiral anomaly: phases of collective excitations and instabilities*, *Phys. Rev. D* **100** (2019) 065023 [[arXiv:1711.08450](https://arxiv.org/abs/1711.08450)] [[INSPIRE](#)].

- [17] I.A. Shovkovy, D.O. Rybalka and E.V. Gorbar, *The overdamped chiral magnetic wave*, *PoS Confinement2018* (2018) 029 [[arXiv:1811.10635](#)] [[INSPIRE](#)].
- [18] M.J. Landry and H. Liu, *A systematic formulation of chiral anomalous magnetohydrodynamics*, [arXiv:2212.09757](#) [[INSPIRE](#)].
- [19] S. Grienering and D.E. Kharzeev, *Spacetime dynamics of chiral magnetic currents in a hot non-Abelian plasma*, *Phys. Rev. D* **108** (2023) 126004 [[arXiv:2308.14825](#)] [[INSPIRE](#)].
- [20] S. Grienering and S. Morales-Tejera, *Real-time dynamics of axial charge and chiral magnetic current in a non-Abelian expanding plasma*, *Phys. Rev. D* **108** (2023) 126010 [[arXiv:2308.14829](#)] [[INSPIRE](#)].
- [21] A. Amoretti et al., *Relaxation terms for anomalous hydrodynamic transport in Weyl semimetals from kinetic theory*, *JHEP* **02** (2024) 071 [[arXiv:2309.05692](#)] [[INSPIRE](#)].
- [22] N.P. Armitage, E.J. Mele and A. Vishwanath, *Weyl and Dirac Semimetals in Three Dimensional Solids*, *Rev. Mod. Phys.* **90** (2018) 015001 [[arXiv:1705.01111](#)] [[INSPIRE](#)].
- [23] A.D. Gallegos and U. Gürsoy, *Dynamical gauge fields and anomalous transport at strong coupling*, *JHEP* **05** (2019) 001 [[arXiv:1806.07138](#)] [[INSPIRE](#)].
- [24] A.A. Burkov, *Negative longitudinal magnetoresistance in Dirac and Weyl metals*, [arXiv:1505.01849](#) [[DOI:10.1103/PhysRevB.91.245157](#)].
- [25] S.Y. Xu et al., *Discovery of a Weyl Fermion semimetal and topological Fermi arcs*, *Science* **349** (2015) 613 [[arXiv:1502.03807](#)] [[INSPIRE](#)].
- [26] B.Q. Lv et al., *Observation of Weyl nodes in TaAs*, [arXiv:1503.09188](#) [[DOI:10.1038/nphys3426](#)].
- [27] K. Landsteiner, Y. Liu and Y.-W. Sun, *Negative magnetoresistivity in chiral fluids and holography*, *JHEP* **03** (2015) 127 [[arXiv:1410.6399](#)] [[INSPIRE](#)].
- [28] A. Lucas, R.A. Davison and S. Sachdev, *Hydrodynamic theory of thermoelectric transport and negative magnetoresistance in Weyl semimetals*, *Proc. Nat. Acad. Sci.* **113** (2016) 9463 [[arXiv:1604.08598](#)] [[INSPIRE](#)].
- [29] P.O. Sukhachov, V.A. Miransky, I.A. Shovkovy and E.V. Gorbar, *Collective excitations in Weyl semimetals in the hydrodynamic regime*, *J. Phys. Condens. Matter* **30** (2018) 275601 [[arXiv:1802.10110](#)] [[INSPIRE](#)].
- [30] W. Gao et al., *Photonic Weyl degeneracies in magnetized plasma*, *Nature Commun.* **7** (2016) 12435 [[arXiv:1511.04875](#)].
- [31] K. Landsteiner and Y. Liu, *The holographic Weyl semi-metal*, *Phys. Lett. B* **753** (2016) 453 [[arXiv:1505.04772](#)] [[INSPIRE](#)].
- [32] K. Landsteiner, Y. Liu and Y.-W. Sun, *Quantum phase transition between a topological and a trivial semimetal from holography*, *Phys. Rev. Lett.* **116** (2016) 081602 [[arXiv:1511.05505](#)] [[INSPIRE](#)].
- [33] E.-G. Moon, C. Xu, Y.B. Kim and L. Balents, *Non-Fermi liquid and topological states with strong spin-orbit coupling*, *Phys. Rev. Lett.* **111** (2013) 206401 [[arXiv:1212.1168](#)] [[INSPIRE](#)].
- [34] I.F. Herbut and L. Janssen, *Topological Mott insulator in three-dimensional systems with quadratic band touching*, *Phys. Rev. Lett.* **113** (2014) 106401 [[arXiv:1404.5721](#)] [[INSPIRE](#)].
- [35] L. Janssen and I.F. Herbut, *Phase diagram of electronic systems with quadratic Fermi nodes in $2 < d < 4$: $2 + \epsilon$ expansion, $4 - \epsilon$ expansion, and functional renormalization group*, *Phys. Rev. B* **95** (2017) 075101 [[arXiv:1611.04594](#)] [[INSPIRE](#)].

- [36] S. Tchoumakov and W. Witczak-Krempa, *Dielectric and electronic properties of three-dimensional Luttinger semimetals with a quadratic band touching*, *Phys. Rev. B* **100** (2019) 075104 [[arXiv:1904.00090](#)].
- [37] S.M. Girvin and K. Yang, *Modern condensed matter physics*, Cambridge University Press (2019) [[DOI:10.1017/9781316480649](#)].
- [38] E. Witten, *Multitrace operators, boundary conditions, and AdS/CFT correspondence*, [hep-th/0112258](#) [[INSPIRE](#)].
- [39] M. Berkooz, A. Sever and A. Shomer, *‘Double trace’ deformations, boundary conditions and space-time singularities*, *JHEP* **05** (2002) 034 [[hep-th/0112264](#)] [[INSPIRE](#)].
- [40] D. Marolf and S.F. Ross, *Boundary Conditions and New Dualities: Vector Fields in AdS/CFT*, *JHEP* **11** (2006) 085 [[hep-th/0606113](#)] [[INSPIRE](#)].
- [41] O. Domenech et al., *Emergent Gauge Fields in Holographic Superconductors*, *JHEP* **08** (2010) 033 [[arXiv:1005.1776](#)] [[INSPIRE](#)].
- [42] M. Montull, O. Pujolas, A. Salvio and P.J. Silva, *Flux Periodicities and Quantum Hair on Holographic Superconductors*, *Phys. Rev. Lett.* **107** (2011) 181601 [[arXiv:1105.5392](#)] [[INSPIRE](#)].
- [43] U. Gran, M. Tornsö and T. Zingg, *Plasmons in Holographic Graphene*, *SciPost Phys.* **8** (2020) 093 [[arXiv:1804.02284](#)] [[INSPIRE](#)].
- [44] E. Mauri and H.T.C. Stoof, *Screening of Coulomb interactions in Holography*, *JHEP* **04** (2019) 035 [[arXiv:1811.11795](#)] [[INSPIRE](#)].
- [45] Y. Ahn et al., *Holography and magnetohydrodynamics with dynamical gauge fields*, *JHEP* **02** (2023) 012 [[arXiv:2211.01760](#)] [[INSPIRE](#)].
- [46] H.-S. Jeong, M. Baggioli, K.-Y. Kim and Y.-W. Sun, *Collective dynamics and the Anderson-Higgs mechanism in a bona fide holographic superconductor*, *JHEP* **03** (2023) 206 [[arXiv:2302.02364](#)] [[INSPIRE](#)].
- [47] M. Baggioli, *How to sit Maxwell and Higgs on the boundary of Anti-de Sitter*, *JHAP* **3** (2023) 1 [[arXiv:2303.10305](#)] [[INSPIRE](#)].
- [48] M. Natsuume and T. Okamura, *Holographic Meissner effect*, *Phys. Rev. D* **106** (2022) 086005 [[arXiv:2207.07182](#)] [[INSPIRE](#)].
- [49] L.V. Delacrétaz, D.M. Hofman and G. Mathys, *Superfluids as Higher-form Anomalies*, *SciPost Phys.* **8** (2020) 047 [[arXiv:1908.06977](#)] [[INSPIRE](#)].
- [50] C. Zhang et al., *Signatures of the Adler-Bell-Jackiw chiral anomaly in a Weyl Fermion semimetal*, *Nature Commun.* **7** (2016) 0735 [[arXiv:1601.04208](#)] [[INSPIRE](#)].
- [51] M. Baggioli, M. Vasin, V.V. Brazhkin and K. Trachenko, *Gapped momentum states*, *Phys. Rept.* **865** (2020) 1 [[arXiv:1904.01419](#)] [[INSPIRE](#)].
- [52] C. Yang, M.T. Dove, V.V. Brazhkin and K. Trachenko, *Emergence and evolution of the k gap in spectra of liquid and supercritical states*, *Phys. Rev. Lett.* **118** (2017) 215502.
- [53] S. Grozdanov, D.M. Hofman and N. Iqbal, *Generalized global symmetries and dissipative magnetohydrodynamics*, *Phys. Rev. D* **95** (2017) 096003 [[arXiv:1610.07392](#)] [[INSPIRE](#)].
- [54] K. Landsteiner, Y. Liu and Y.-W. Sun, *Holographic topological semimetals*, *Sci. China Phys. Mech. Astron.* **63** (2020) 250001 [[arXiv:1911.07978](#)] [[INSPIRE](#)].
- [55] A. Jimenez-Alba, K. Landsteiner, Y. Liu and Y.-W. Sun, *Anomalous magnetoconductivity and relaxation times in holography*, *JHEP* **07** (2015) 117 [[arXiv:1504.06566](#)] [[INSPIRE](#)].

- [56] X. Li, B. Roy and S. Das Sarma, *Weyl fermions with arbitrary monopoles in magnetic fields: Landau levels, longitudinal magnetotransport, and density-wave ordering*, *Phys. Rev. B* **94** (2016) 195144 [[arXiv:1608.06632](#)] [[INSPIRE](#)].
- [57] R.C.L. Bruni, L.F. Ferreira and D.M. Rodrigues, *Magnetic-field-driven topological phase transition in the holographic Weyl semimetal*, *Phys. Rev. D* **108** (2023) 066010 [[arXiv:2303.11992](#)] [[INSPIRE](#)].
- [58] D. Colladay and V.A. Kostelecky, *Lorentz violating extension of the standard model*, *Phys. Rev. D* **58** (1998) 116002 [[hep-ph/9809521](#)] [[INSPIRE](#)].
- [59] Y.-W. Sun and Q. Yang, *Negative magnetoresistivity in holography*, *JHEP* **09** (2016) 122 [[arXiv:1603.02624](#)] [[INSPIRE](#)].
- [60] U. Gran, M. Tornsö and T. Zingg, *Holographic Plasmons*, *JHEP* **11** (2018) 176 [[arXiv:1712.05672](#)] [[INSPIRE](#)].
- [61] M. Baggioli, Y. Bu and V. Ziogas, *U(1) quasi-hydrodynamics: Schwinger-Keldysh effective field theory and holography*, *JHEP* **09** (2023) 019 [[arXiv:2304.14173](#)] [[INSPIRE](#)].
- [62] M. Baggioli and K. Trachenko, *Maxwell interpolation and close similarities between liquids and holographic models*, *Phys. Rev. D* **99** (2019) 106002 [[arXiv:1808.05391](#)] [[INSPIRE](#)].
- [63] M. Baggioli and K. Trachenko, *Low frequency propagating shear waves in holographic liquids*, *JHEP* **03** (2019) 093 [[arXiv:1807.10530](#)] [[INSPIRE](#)].
- [64] U. Gran, M. Tornsö and T. Zingg, *Exotic Holographic Dispersion*, *JHEP* **02** (2019) 032 [[arXiv:1808.05867](#)] [[INSPIRE](#)].
- [65] M. Baggioli et al., *Holographic Plasmon Relaxation with and without Broken Translations*, *JHEP* **09** (2019) 013 [[arXiv:1905.00804](#)] [[INSPIRE](#)].
- [66] M. Baggioli, U. Gran and M. Tornsö, *Transverse Collective Modes in Interacting Holographic Plasmas*, *JHEP* **04** (2020) 106 [[arXiv:1912.07321](#)] [[INSPIRE](#)].
- [67] M. Baggioli, U. Gran and M. Tornsö, *Collective modes of polarizable holographic media in magnetic fields*, *JHEP* **06** (2021) 014 [[arXiv:2102.09969](#)] [[INSPIRE](#)].
- [68] Y. Liu and Y.-W. Sun, *Topological nodal line semimetals in holography*, *JHEP* **12** (2018) 072 [[arXiv:1801.09357](#)] [[INSPIRE](#)].
- [69] Y. Liu and X.-M. Wu, *An improved holographic nodal line semimetal*, *JHEP* **05** (2021) 141 [[arXiv:2012.12602](#)] [[INSPIRE](#)].
- [70] R. Rodgers, E. Mauri, U. Gürsoy and H.T.C. Stoof, *Thermodynamics and transport of holographic nodal line semimetals*, *JHEP* **11** (2021) 191 [[arXiv:2109.07187](#)] [[INSPIRE](#)].
- [71] M. Kaminski, C.F. Uhlemann, M. Bleicher and J. Schaffner-Bielich, *Anomalous hydrodynamics kicks neutron stars*, *Phys. Lett. B* **760** (2016) 170 [[arXiv:1410.3833](#)] [[INSPIRE](#)].
- [72] S. Hanai and N. Yamamoto, *Chiral asteroseismology: seismic oscillations caused by chiral transport in neutron stars and supernovae*, *JCAP* **10** (2023) 018 [[arXiv:2203.16133](#)] [[INSPIRE](#)].
- [73] M. Giovannini and M.E. Shaposhnikov, *Primordial hypermagnetic fields and triangle anomaly*, *Phys. Rev. D* **57** (1998) 2186 [[hep-ph/9710234](#)] [[INSPIRE](#)].
- [74] K. Kamada, N. Yamamoto and D.-L. Yang, *Chiral effects in astrophysics and cosmology*, *Prog. Part. Nucl. Phys.* **129** (2023) 104016 [[arXiv:2207.09184](#)] [[INSPIRE](#)].
- [75] S. Xue et al., *Electronic collective excitations in topological semimetals*, *Prog. Surf. Sci.* **98** (2023) 100719.

- [76] M.N. Chernodub and M.A.H. Vozmediano, *Chiral sound waves in strained Weyl semimetals*, *Phys. Rev. Res.* **1** (2019) 032040 [[arXiv:1904.09113](#)] [[INSPIRE](#)].
- [77] M. Baggioli, M.N. Chernodub, K. Landsteiner and M.A.H. Vozmediano, *Detect Axial Gauge Fields with a Calorimeter*, *SciPost Phys. Core* **3** (2020) 013 [[arXiv:2004.02473](#)] [[INSPIRE](#)].
- [78] M. Baggioli and B. Goutéraux, *Colloquium: Hydrodynamics and holography of charge density wave phases*, *Rev. Mod. Phys.* **95** (2023) 011001 [[arXiv:2203.03298](#)] [[INSPIRE](#)].